Diagnostics of magnetospheric electron density and irregularities at altitudes <5000 km using whistler and Z mode echoes from radio sounding on the IMAGE satellite

V. S. Sonwalkar,[1] D. L. Carpenter,[2] T. F. Bell,[2] M. Spasojević,[2,3] U. S. Inan,[2] J. Li,[1] X. Chen,[1] A. Venkatasubramanian,[1] J. Harikumar,[4,5] R. F. Benson,[6] W. W. L. Taylor,[7] and B. W. Reinisch[8]

Received 10 March 2004; revised 14 June 2004; accepted 5 August 2004; published 16 November 2004.

[1] When the Radio Plasma Imager (RPI) on the IMAGE satellite operates in the inner plasmasphere and at moderate to low altitudes over the polar regions, pulses emitted at the low end of its 3-kHz to 3-MHz sounding frequency range can propagate in the whistler mode and/or in the Z mode. During soundings with both 25.6-ms pulses and 3.2-ms pulses, whistler mode echoes have been observed in (1) ''discrete,'' lightning whistler–like forms and (2) diffuse, widely time spread forms suggestive of mode coupling at the boundaries of density irregularities. Discrete echoes have been observed at altitudes less than ≈5000 km both inside the plasmasphere and over the auroral and polar regions, being most common inside the plasmasphere. Diffuse echoes have also been observed at altitudes less than 5000 km, being most common poleward of the plasmasphere. Either discrete or diffuse echoes or both have been detected during one or more soundings on at least half of all IMAGE orbits. In regions poleward of the plasmasphere, diffuse Z mode echoes of a kind reported by Carpenter et al. (2003) were found to accompany both discrete and diffuse whistler mode echoes 90% of the time and were also present during 90% of the soundings when no whistler mode echoes were detected. It is proposed that the observed discrete whistler mode echoes are a consequence of RPI signal reflections at the bottom side of the ionosphere and that diffuse whistler mode echoes are a result of scattering of RPI signals by geomagnetic field-aligned electron density irregularities located within 2000 km earthward of the satellite and in directions close to that of the field line passing through IMAGE. Diffuse Z mode echoes are believed to be due to scattering of RPI signals from electron density irregularities within 3000 km of the satellite, particularly those in the generally cross-**B** direction. Consistent with previous works, our results indicate that the magnetosphere at high latitudes is highly structured, with electron density irregularities that exist over cross-**B** scales ranging from 10 m to 100 km and that profoundly affect whistler mode propagation. It is demonstrated that both kinds of whistler mode echoes as well as diffuse Z mode echoes have potential for local and remote diagnostics of electron density distributions and structures. *INDEX TERMS:* 2403 Ionosphere: Active experiments; 2772 Magnetospheric Physics: Plasma waves and instabilities; 2794 Magnetospheric Physics: Instruments and techniques; 2439 Ionosphere: Ionospheric irregularities; 2481 Ionosphere: Topside ionosphere; *KEYWORDS:* Whistler mode echoes, Z mode echoes, whistler and Z mode wave injection, plasma waves, plasma density irregularities, whistler and Z mode sounding

Citation: Sonwalkar, V. S., et al. (2004), Diagnostics of magnetospheric electron density and irregularities at altitudes <5000 km using whistler and Z mode echoes from radio sounding on the IMAGE satellite, *J. Geophys. Res.*, *109*, A11212, doi:10.1029/2004JA010471.

[1]Electrical and Computer Engineering Department, University of Alaska Fairbanks, Fairbanks, Alaska, USA.
[2]Space, Telecommunications, and Radioscience Laboratory, Stanford University, Stanford, California, USA.
[3]Now at Space Physics Research Group, Space Science Laboratory, University of California, Berkeley, California, USA.
[4]Space Data Systems, Los Alamos National Laboratory, Los Alamos, New Mexico, USA.
[5]Now at Physical Science Laboratory, New Mexico State University, Las Cruces, New Mexico, USA.
[6]NASA Goddard Space Flight Center, Greenbelt, Maryland, USA.
[7]QSS Group, Inc., NASA Goddard Space Flight Center, Greenbelt, Maryland, USA.
[8]Center for Atmospheric Research, University of Massachusetts, Lowell, Massachusetts, USA.

0148-0227/04/2004JA010471$09.00

1. Introduction

[2] The Radio Plasma Imager (RPI) on the IMAGE satellite (1000 km × 7.2 R_E altitude polar orbit) was designed to use the classical radio sounding technique at geocentric distances up to ≈8 R_E [*Reinisch et al.*, 2000; *Burch*, 2000]. The sounding frequency range was extended downward from 3 MHz to 3 kHz to permit determination of the electron density n_e in outer magnetospheric plasmas as tenuous as n_e = 0.1 cm^{-3} and the reception of echoes from remote plasma regions with $10 < n_e < 10^5$ cm^{-3}. In planning the experiments it was realized that signals transmitted at frequencies below either the local plasma frequency f_{pe} or gyrofrequency f_{ce}, whichever is lower, could propagate in the whistler mode, and that Z mode echoes could be excited in a band below the local upper hybrid frequency f_{uh}. The whistler and Z modes are called "trapped" modes, as opposed to "free space" modes, because of the upper frequency limits on their local propagation imposed by the dispersion relations for wave propagation in plasmas [e.g., *Budden*, 1985]. Figures 1a and 1b are dispersion diagrams, plots of frequency $f = \omega/2\pi$ versus wave number k, that illustrate schematically the relationship between the trapped modes and the free space ordinary and extraordinary (O and X) modes used in conventional radio sounding. Figure 1a represents the condition $f_{pe}/f_{ce} > 1$, which is common below ≈2000 km and above ≈4000 km within the Earth's plasmasphere, while Figure 1b represents the condition $f_{pe}/f_{ce} < 1$, which regularly prevails over a wide range of altitudes in regions poleward of the plasmapause.

[3] A key difference between the free space O and X modes and the whistler and Z modes is in the phase velocity, expressed as $2\pi f/k \equiv \omega/k$, which exceeds the speed of light in vacuum for the O and X modes but is subluminous for the whistler mode and the right-hand-polarized branch of the Z mode at frequencies above f_{pe}. The whistler mode and right-hand-polarized Z mode are therefore capable of strong resonant interactions with the hot electron plasmas of the magnetosphere.

[4] The operation of a whistler mode transmitter in the magnetosphere has been an unrealized goal of space scientists for many years. Interest in a spaceborne transmitter project was stimulated by ground-based whistler mode wave injection experiments from Antarctica which showed that relatively weak (a few watts radiated power) coherent signals injected into the outer plasmasphere at frequencies between 2 kHz and 6 kHz could experience wave growth by 30 dB and be received at a conjugate ground station [*Helliwell and Katsufrakis*, 1974, 1978].

[5] In the late 1970s a NASA study group was formed to consider active wave experiments from the Shuttle [e.g., *Fredricks et al.*, 1978; *Dyson*, 1978; *Inan et al.*, 1981]. This group and its successor developed plans for a wave injection mission called WISP, to include a transmitter on the Shuttle and signal detection on a subsatellite. The project was selected for a Shuttle flight in the mid 1980s but was cancelled after the Challenger accident in 1986.

[6] Scientists in Russia and the former USSR also sought to implement whistler mode wave injection experiments. The low-altitude AKTIVNY satellite, launched in 1990, carried an inflatable loop antenna but was unsuccessful in producing detectable whistler mode signals, possibly due to a failure of the antenna to deploy correctly [e.g., *Sonwalkar et al.*, 1994]. It was reported, however, that the antenna excited electrostatic turbulence close to the ACTIVNY satellite [*Molchanov et al.*, 1997].

[7] Once IMAGE moved into the development phases, its broad potential for whistler mode probing became clear. It was pointed out that in major parts of the plasmasphere the whistler mode refractive index is high, of order 10, and the long RPI antennas are approximately a half wavelength in extent and can have a radiation efficiency at whistler mode frequencies of as much as 10% [e.g., *Sonwalkar et al.*, 2001], much higher than when, usually at much higher altitudes, radiation at those same frequencies is in the free space modes. In the latter case, the efficiency of the antennas drops steeply with decreasing frequency below 100 kHz from a maximum near 200–300 kHz [*Reinisch et al.*, 2000].

[8] At the time of IMAGE launch, there were a number of questions about prospects for whistler mode detection. First of all, an antenna tuning network developed for antenna impedance control would be in regular use [*Reinisch et al.*, 2000]. Under free space conditions, the antenna impedance would be mainly capacitive for f < 300 kHz; hence various combinations of switchable inductors and tuning capacitors would be used to minimize the reactance at a set of approximately logarithmically spaced frequencies extending up to ≈300 kHz. Above that frequency the reactance would be primarily inductive, and switchable capacitors would be used for tuning [*Reinisch et al.*, 2000]. Under whistler mode conditions this antenna tuning would not be ideal; because of the antenna sheath capacitance, larger inductors would generally be needed for impedance control at particular frequencies below 300 kHz (the half-wave resonance frequency of the long antennas in free space), while above 300 kHz, inductors, and not the planned capacitors, would be desirable.

[9] Secondly, would detectable whistler mode echoes be produced during sounding with short, 3.2-ms pulses, either with or without the use of coherent integration? At frequencies greater than about 10 kHz, such pulses might experience substantial spreading losses as well as ionospheric attenuation because, as discussed below, they must travel back and forth along paths from IMAGE to reflection points along the bottom side of the ionosphere. In past ionospheric topside sounding work, whistler mode echoes were relatively rare, being confined for the most part to frequencies below 800 kHz, at which the power output of the sounders was relatively low. *Muldrew* [1969] reported reception on Alouette 2 of whistler mode echoes in a band from the sounder's low-frequency limit of 200 kHz up to 850 kHz. The echoes occurred on a limited number of ionograms acquired at high latitudes in early morning. The author interpreted these echoes as having reflected at the Earth's surface after undergoing conversion to the right-hand-polarized extraordinary mode at a lower-ionosphere altitude near or below 100 km where the wave frequency equals f_{pe}.

[10] Introductory announcements about whistler mode echoes from RPI were made by *Sonwalkar et al.* [2000] and *Fung et al.* [2003]. In this paper we describe discrete

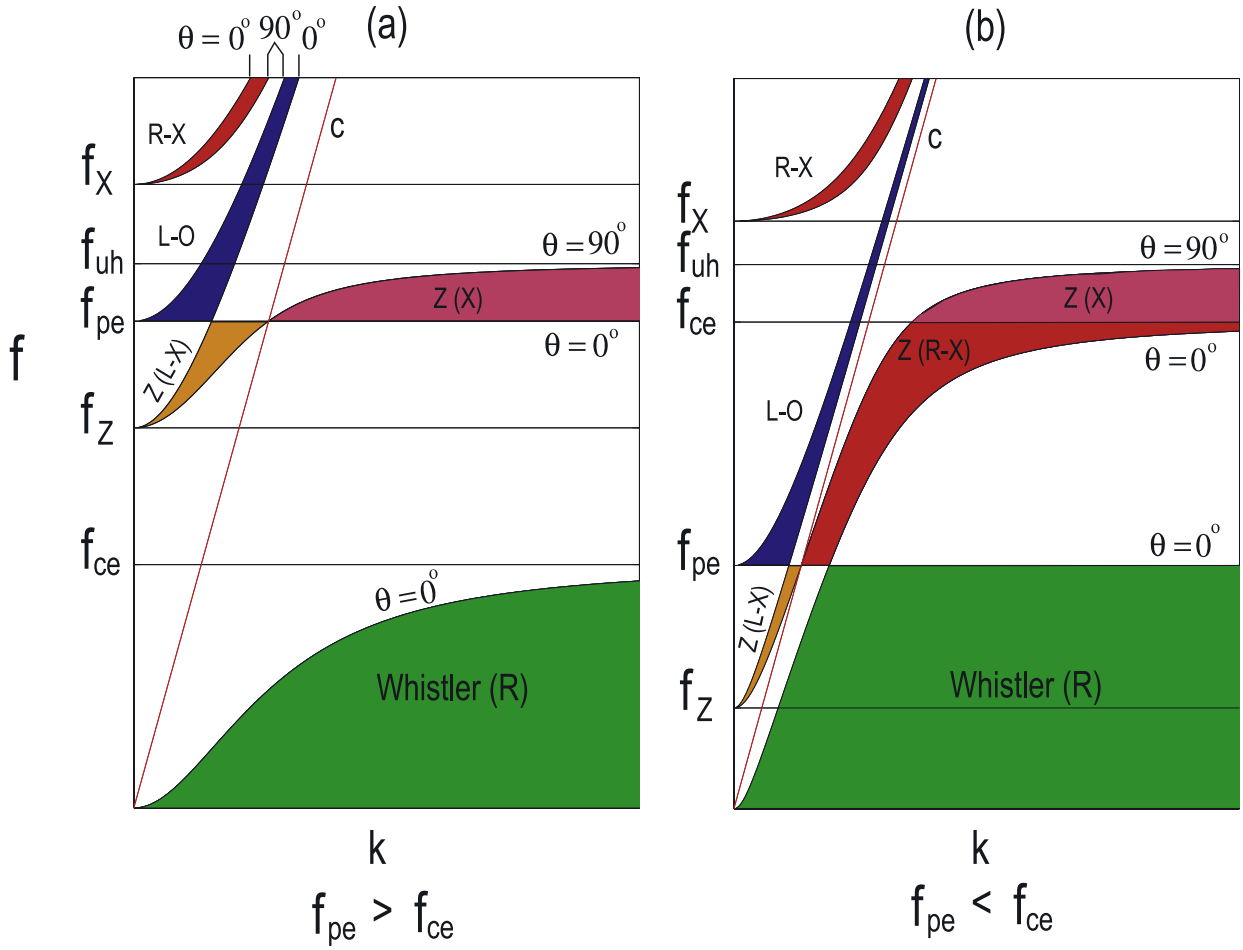

Figure 1. Dispersion diagrams, in coordinates of wave frequency f versus wave number k, showing regions of oblique propagation in various modes for a two-component (electron and proton) cold plasma. (a) Diagram for the case of electron plasma frequency f_{pe} greater than the electron gyrofrequency f_{ce}, a situation common within the plasmasphere. The band of no propagation between f_Z and f_{ce} appears only when f_{pe}/f_{ce} exceeds $\sqrt{2}$. (b) Diagram for the case of $f_{ce} > f_{pe}$, a situation common poleward of the plasmapause. Adapted from *Goertz and Strangeway* [1995].

and diffuse whistler mode echoes that have been detected on many occasions during routine RPI sounding operations with 3.2-ms pulses, both with and without the use of coherent integration. We then discuss the conditions of occurrence of the echoes and conclude with an illustration of the use of the echoes for measurement of low- to medium-altitude electron density and structure in the magnetosphere. We also discuss and illustrate the diagnostic potential of certain diffuse Z mode echoes that are almost always present on RPI records from locations where $f_{pe}/f_{ce} < 1$. An overview of RPI Z mode echoes is presented in a paper by *Carpenter et al.* [2003].

2. Instrument Description

[11] RPI is a multimode instrument [*Reinisch et al.*, 2000] in which sounding and listening frequencies, range detection, pulse characteristics and repetition rate are adjustable parameters over a wide range of values. The instrument covers the frequency range from 3 kHz to 3 MHz with a receiver bandwidth of 300 Hz. There are three orthogonal thin wire antennas, two 500-m tip-to-tip dipoles in the spin plane (X and Y) and a 20-m tip-to-tip dipole along the spin axis (Z). The long dipoles are used for transmission, and all three antennas are used for reception. The nominal radiated power from RPI, variable (in terms of free space mode excitation) from 0.1 mW at low frequencies to ≈10 W per dipole at 200 kHz, was reduced by 3 dB on 8 May 2000 when the power supply for the y-axis transmitter failed. A further reduction occurred on 3 October 2000, when one of the x-axis monopoles was partially severed, apparently by a micrometeorite, reducing the dipole length to 340 m. On 18 September 2001 an unknown (presumably small and negligible) section of the Y antenna was lost. In spite of these difficulties, excellent data have continued to be acquired, as described below.

[12] Having been designed as a sounder, RPI (as already noted) is far from ideal for whistler mode applications, being limited to a receiver bandwidth of 300 Hz and during most regular sounding operations to pulses of 3.2-ms duration. There are compensating factors, however, such as the availability of a 500-m dipole antenna for transmis-

sion (now reduced to ≈340 m) and crossed 500-m antennas (one ≈340 m) and a 20-m Z antenna for reception.

3. Observations of Whistler Mode Echoes

3.1. Problem of Whistler Mode Echo Detection

[13] The cancelled Shuttle wave injection mission noted above included a subsatellite. Lacking such a remote receiver, RPI has been forced to depend upon the special conditions under which whistler mode echoes of its signals can be received. Three such conditions are envisaged [*Sonwalkar et al.*, 2001]. In the magnetospheric reflection, or MR, process, the direction of a downgoing ray is reversed when the wave frequency becomes equal to the local value of the lower hybrid resonance frequency f_{lh}. At f_{lh}, which is a function of f_{pe}, f_{ce}, and the effective mass of the ions [e.g., *Stix*, 1962; *Brice and Smith*, 1965] the refractive index surface undergoes a transition from an open (with a resonance cone) to a closed topology [e.g., *Smith and Angerami*, 1968]. The MR process is limited to frequencies less than the maximum value of f_{lh} in the ionosphere, ≈12 kHz.

[14] In the second case, downgoing waves undergo a Snell's law type of reflection from the steep vertical density gradients near 90 km in the lower ionosphere [*Helliwell*, 1965]. Echoes of stepped frequencies should then in principle exhibit lightning whistler–like forms on plots of frequency versus time delay when RPI is operating along certain near-Earth portions of the IMAGE orbit.

[15] The third case involves a two-stage process: downgoing RPI whistler mode signals initially encounter small-scale field-aligned density irregularities (10 m to several 100 m in the cross-**B** direction, where **B** is the geomagnetic field). The signals can then be strongly coupled by either linear and nonlinear mechanisms into quasi-electrostatic whistler mode waves (lower hybrid waves) with wavelengths of the same order of magnitude as the spatial wavelength of the irregularities [*Bell and Ngo*, 1988; *Titova et al.*, 1984; *Groves et al.*, 1988; *Tanaka et al.*, 1987; *Ohnami et al.*, 1993]. This coupling generally produces downward propagating lower hybrid waves, but these waves can be partially reflected upward as they further encounter the small-scale density structure in the medium. Echoes generated by this two-stage process are expected to contain large wave normal angles close to the whistler mode resonance cone, and hence should exhibit substantial spreading in group delay.

[16] In the data examined thus far we have not detected echoes that can be attributed to the MR-type reflection process, probably because most of the transmitted signals were at frequencies above the maximum f_{lh} (≈12 kHz) in the magnetosphere and/or because the transmission efficiency below 10–12 kHz was poor because of inadequate coupling of transmitter energy to the antenna for the whistler mode, as discussed earlier. On the other hand, we have found many cases of echoes whose properties are consistent either with reflections by the steep density gradient in the lower ionosphere or with scattering by small irregularities. Echoes apparently resulting from ionospheric reflection regularly exhibit a discrete trace on a record of frequency versus time delay, analogous to that of a lightning-generated whistler, while those apparently resulting from scattering tend to exhibit a wide and irregular range of delays. We present below examples of these two types of echo and also discuss a type of Z mode echo that regularly occurs in the region poleward of the plasmapause and is believed to be the result of scattering from irregularities.

3.2. Examples of Discrete Echoes With Minimal Spreading in Time Delays at Each Frequency

[17] During typical RPI operations, a sounding program lasting from tens to hundreds of seconds is repeated at intervals of 2 to 10 min within a schedule containing other programs and passive recordings [*Reinisch et al.*, 2000]. In May 2002 a program consisting of 3.2-ms sequentially transmitted pulses at 144 logarithmic frequency steps between 60 and 1000 kHz was in operation. Figures 2a and 2b show plasmagrams displaying whistler mode echoes received on 20 and 21 May 2002, respectively. An RPI plasmagram normally plots the virtual range of echoes in Earth radii (R_E) as a function of sounding frequency [*Galkin et al.*, 2001], with virtual range calculated from the measured time delay assuming that the signal has propagated at the velocity of light in free space. However, in this paper we will display the echo time delay in milliseconds instead of virtual range, since whistler mode group velocities and most Z mode group velocities are substantially lower than c, and since in the whistler mode literature elapsed time from a specific reference point is commonly presented, especially for transient events. In Figures 2a and 2b, there is a minimum observable time delay of 13 ms because of the 3.2-ms minimum transmitted pulse length and additional time needed for the receiver to recover from the high voltage generated during the transmitter pulses. Amplitude is color coded in units of dB nV m^{-1} (dB relative to a 1 nV m^{-1} input signal).

[18] The whistler mode (WM) echoes in Figures 2a and 2b are the traces below ≈300 kHz. Echoes such as these with narrowly defined time delay as a function of frequency are called discrete echoes. In these cases the echoes covered one or two 3.2-ms range bins at each frequency (temporal resolution imposed by the pulse length is 3.2 ms). In Figure 2c, the plasmagram of Figure 2a is shown with the axes interchanged, a format commonly used to show natural whistler mode activity. Figure 2d shows a plot of the low-altitude portion of the IMAGE polar orbit for the case of Figure 2a.

[19] In Figures 2a, 2b, and 2c the signals above ≈300 kHz with time delay spread that increases with frequency are diffuse Z mode (ZM) echoes. As discussed by *Carpenter et al.* [2003], this pattern is characteristic of the low-altitude polar region and the plasma condition $f_{pe}/f_{ce} < 1$ illustrated in Figure 1b. The abrupt high-frequency cutoff of the Z mode echoes, and of the long-duration sounder-stimulated plasma resonance at ≈787 kHz in Figures 2a and 2c, provides a measure of the upper hybrid resonance frequency f_{uh} [*Benson et al.*, 2003], while the gap or decrease in echo spreading at ≈685 kHz provides a measure of the local f_{ce} [*Carpenter et al.*, 2003]. From these parameters the plasma frequency f_{pe} in this case is calculated to be ≈387 kHz, since $f_{uh}^2 = f_{pe}^2 + f_{ce}^2$.

[20] The echoes below 300 kHz in Figure 2 are identified as whistler mode because: (1) they are confined to frequencies below the lower of f_{pe} and f_{ce} (≈387 kHz and 685 kHz,

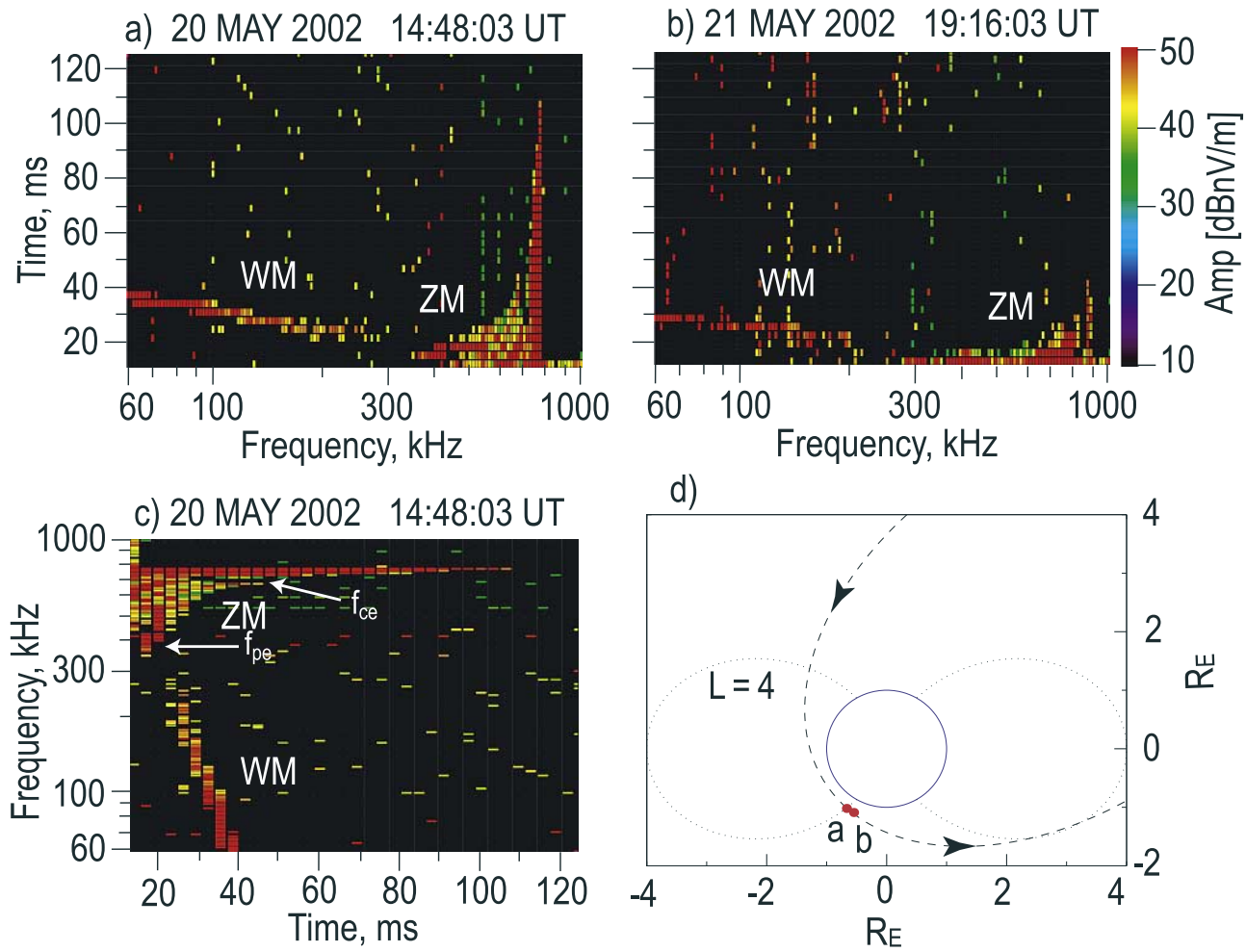

Figure 2. Examples of whistler mode echoes received during soundings by RPI in May 2002. (a–b). Plasmagrams displaying time delay versus frequency for whistler mode echoes received on 20 May and 21 May 2002. The whistler mode echoes are the discrete traces below ≈300 kHz. Echoes above ≈300 kHz showing a spread in time delay at each frequency are identified as Z mode echoes. A noise suppression algorithm [*Galkin et al.*, 2001] was used in processing the data. (c) The whistler mode echo of 20 May 2002 in Figure 2a is shown in a format displaying frequency versus time delay, an interchange of the axes of the plasmagram presentation shown in Figures 2a and 2b. (d) Plot of the low-altitude portion of the IMAGE polar orbit for the case of Figure 2a. The approximate locations of IMAGE for the two cases are indicated by red dots. Dipole field lines at $L = 4$ are shown as a reference. The magnetic local times for the cases in Figures 2a and 2b were 9.35 and 10.81, respectively.

respectively, for 2a); (2) they show an increase in delay with decreasing frequency (in the case of Figures 2a and 2c, from ≈25 ms to ≈40 ms). These are well known properties of the dispersed impulses from lightning called "whistlers" [e.g., *Helliwell*, 1965; *Hayakawa*, 1995]. In the simplified diagrams of Figure 1, group velocity is $2\pi df/dk \equiv d\omega/dk$; this quantity can be seen to decrease as frequency decreases in the lower portion of the whistler mode region.

[21] We believe that the whistler mode echoes shown in Figure 2 are the result of signal reflections from the bottom side of the ionosphere. The observed echo delays of tens of milliseconds are consistent with observations of the time required for whistler mode waves from lightning to travel twice through the ionosphere [*Carpenter et al.*, 1964].

[22] In this paper we will use the $f - t$ format (as in Figure 2c) to show additional examples of lightning whistler–like behavior, while in cases emphasizing diffuse whistler mode or Z mode echoes, we will return to the conventional *t*-versus-*f* plasmagram style format.

3.3. Discrete Echoes, With Medium Time Delay Spreading, From Successive Soundings

[23] Figure 3 shows frequency-versus-time records of whistler mode echoes received during five successive soundings as IMAGE moved (see Figure 3f) from near perigee in the southern polar region into the duskside plasmasphere. A single 3.2-ms pulse was transmitted at each of 78 frequencies spaced by 900 Hz over the range 180–245 kHz during the sounding program in use at this time. Amplitude is shown in dB(nV/m) as received on the long X antenna. Note the contrast between the soundings previously illustrated in Figure 2, which provide a wide

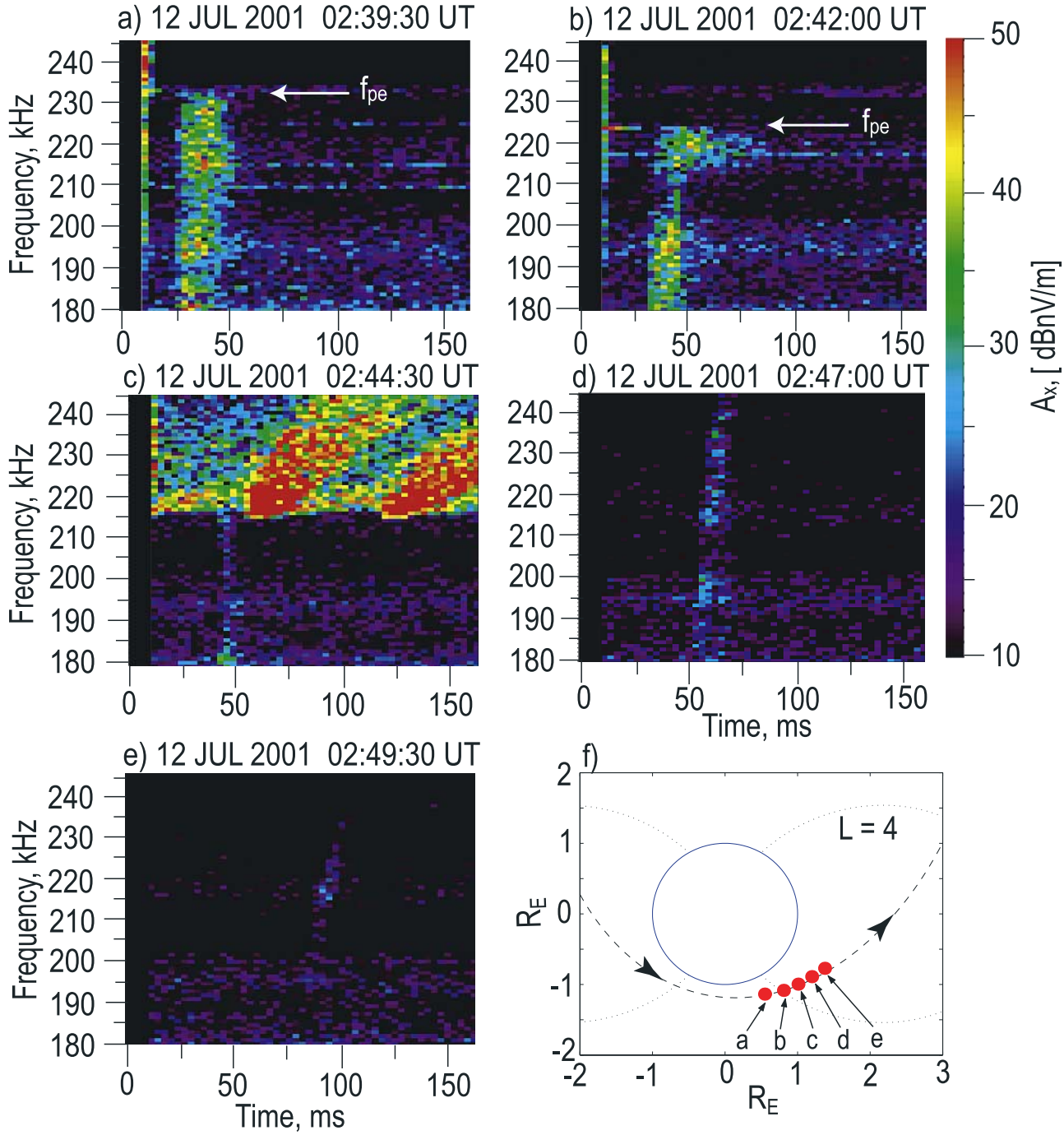

Figure 3. (a–e). Series of $f - t$ plasmagrams showing whistler mode echoes on five successive soundings extending from $L \approx 5.5$ outside the plasmasphere to $L \approx 2.2$ inside the plasmasphere. The data were acquired on 12 July 2001. These echoes, in particular, cases in Figures 3a and 3b, show a range of time delays at each frequency; they are still noticeable, however, as discrete traces on spectrograms. (f) Plot of the low-altitude portion of the IMAGE polar orbit. The approximate locations of IMAGE for cases in Figures 3a–3e are indicated by red dots. Dipole field lines at $L = 4$ are shown as a reference. The magnetic local times for the cases in Figures 3a–3e varied from 18.74 to 18.00.

frequency range survey with logarithmic frequency stepping, and those from Figure 3, which feature linear frequency stepping over a narrow range beginning at 180 kHz, well above the low-frequency limit of Figure 2.

[24] Figure 3a shows data recorded at an altitude of ≈2000 km and at $L \approx 5.5$. There was a strong band of whistler mode echoes with total time spread of ≈20 ms around a mean travel time of ≈40 ms. The mean echo travel time was roughly constant from the lowest measured frequency of 180 kHz to an upper cutoff at 232 kHz.

[25] During the next sounding 2 1/2 min later, illustrated in Figure 3b, the IMAGE altitude was ≈2300 km and the L

value ≈3.7. In this case the amount of time spreading was ≈15 ms total, except near the uppermost frequencies. The apparent upper cutoff was 224 kHz, down from 232 kHz during the previous sounding.

[26] Figure 3c shows the next sounding, at ≈2700 km altitude and $L \approx 2.8$. At this point the spacecraft was in the plasmasphere boundary layer or PBL, a region of transition from the low plasma densities of the polar region to the high densities of the plasmasphere [*Carpenter*, 2004]. Weak whistler mode echoes, strongest near 180 kHz, appeared with a travel time of ≈50 ms and with only ≈10 ms total time spread at most. Above ≈216 kHz the whistler echoes were not visible as they merged with much stronger Z mode echoes of a type that appeared at similar locations in the PBL in the June–July 2001 period. Such Z mode echoes are discussed by *Carpenter et al.* [2003].

[27] The next record, Figure 3d, shows weak whistler mode echoes received at ≈3100 km altitude and $L \approx 2.4$. The echoes were defined over the full frequency range of the record, and travel time exhibited a slight increase with frequency, beginning at a value of ≈60 ms near 180 kHz. This effect continued during the next sounding, shown in Figure 3e for an altitude of ≈3500 km and $L \approx 2.2$. Here the echoes were very weak, from 20 to 30 dB less intense than the example of Figure 3a and limited to frequencies below ≈234 kHz. The travel time increased with frequency from ≈80 ms at 180 kHz to ≈100 ms near 230 kHz.

[28] The echoes in Figure 3 show typical aspects of the changes in whistler mode dispersion characteristics as IMAGE moved from a high-latitude region where $f_{pe}/f_{ce} < 1$ (Figures 3a and 3b) to a plasmasphere region where $f_{pe}/f_{ce} > 1$. The abrupt upper cutoff of the whistler mode echoes in Figures 3a and 3b is interpreted as occurring at f_{pe}. This cutoff and the lack of variation of group delay with frequency within the displayed limits of the records are consistent with the dispersion diagram of Figure 1b. In both Figures 3a and 3b, Z mode echoes may be seen on the left in the first time/range bin at ≈13 ms, extending well down into the whistler mode region, again in accordance with Figure 1b.

[29] Along the 12 July 2001 orbit illustrated in Figure 3f, the transition from the southern polar region to the plasmasphere occurred at approximately the time of Figure 3c. The L value then was ≈2.8, roughly the same as that of a sharp initial factor of ≈3 density drop detected ≈35 minutes later as IMAGE exited the main plasmasphere and entered a highly structured boundary layer region. In Figure 3c, the whistler mode echo was barely discernible above the noise, and was not identifiable above the Z mode cutoff. In contrast the Z mode signals were very strong, consisting of both individual elements and a widely time-spread background.

[30] The echoes of Figures 3d and 3e were recorded under plasma conditions such as those illustrated in Figure 1a, with $f_{pe}/f_{ce} > 1$. The echoes were limited to frequencies below f_{ce}, which dropped from ≈380 kHz at the time of Figure 3c to 304 kHz in Figure 3e. The resonance at f_{ce} gave rise to a "nose" effect, in which echo travel time increased above a frequency of minimum delay. This effect, familiar from lightning whistler records [e.g., *Helliwell*, 1965], became more pronounced in Figure 3e, due to the drop in f_{ce} with increased spacecraft altitude. In a homogeneous plasma, the nose occurs at $f_{ce}/4$ [e.g., *Helliwell*, 1965]. In the case of Figure 3e, its frequency may be estimated as ≈120 kHz, based upon considerations of the integrated effects of propagation through the inhomogeneous ionosphere to an altitude of 3500 km.

[31] The changes in electron density along the IMAGE orbit of Figure 3 are coarsely mirrored by the observed whistler mode group delays, which provide an integral measure of electron density between IMAGE and the underlying bottom side ionosphere. Between the first and second soundings of Figure 3, the fractional increase in group delay was proportional to the increase in altitude, and hence consistent with no substantial spatial change in the electron density profile below the spacecraft. Beginning at the next sounding (Figure 3c), however, the fractional increase in group delay (since the time of Figure 3a) began to exceed that of the path length, so that by the time of Figure 3e, it had reached ≈1.8, implying that the integrated density along the subsatellite path had increased by a factor of ≈3 (the square of 1.8). Meanwhile, data on n_e at the satellite from soundings in various frequency ranges, including those of Figure 3, showed an increase in electron density at the satellite by a factor of ≈5 to 6. The difference between this change and that in the path-integrated density is attributed to latitudinal changes in the shape of the profile of n_e with distance along the field lines.

3.4. Discrete Echoes From Soundings Using Coherent Integration

[32] In the early months of RPI operations, a sounding program was widely used that involved 25.6-ms pulses at 40 frequencies between 10 kHz and 1800 kHz. In contrast to the soundings of Figures 2 and 3, this program involved coherent integration of received signals and coverage below the 60-kHz low-frequency limit of Figure 2. The 40 frequencies were roughly logarithmically spaced at the center frequencies of the coupling circuits designed to tune the antennas for optimum performance (under free space mode conditions). Each 25.6-ms pulse consisted of eight 3.2-ms "chips"; coherent integration was achieved through phase coding of the 8 chips and correlation of the transmitted format with received echoes [*Reinisch et al.*, 2000]. Eight of these coded pulses were transmitted at each of the 40 frequencies, and for each frequency the signals in each range gate were Fourier analyzed to achieve spectral integration.

[33] During these soundings a number of whistler mode echoes were detected at altitudes from ≈1200 to 7000 km along subauroral field lines. The echoes were discrete, with delay times in the 30–100 ms range, and occupied from one to three 3.2-ms range bins at each frequency. Figures 4a–4c show, in coordinates of frequency (linear scale) from 10 kHz to 100 kHz versus echo delay, spectrograms of three examples obtained in early May 2000. Linear amplitude in arbitrary units is displayed. All three events were detected poleward of the plasmapause within the L range 5.0 to 6.5. The minimum observable echo delay was 25.6 ms, due to the combined effects of the transmitted pulse length and the method of signal processing.

[34] Figure 4d is a plot of low-altitude portions of the IMAGE polar orbit for the case of 8 May 2000 (Figure 4a). Dipole field lines at $L = 4$ have been added as a rough

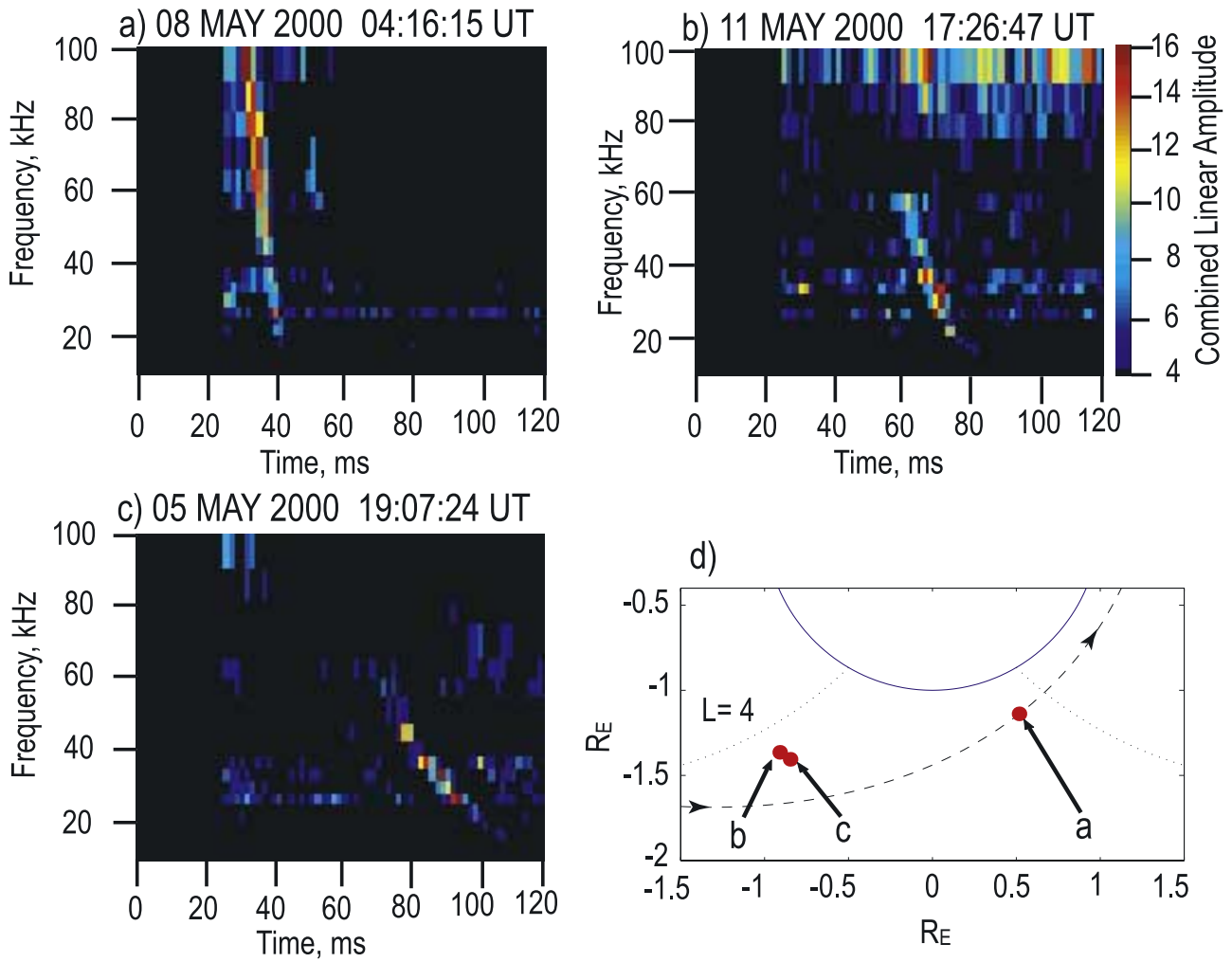

Figure 4. (a–c). Plasmagrams containing examples of whistler mode echoes received during soundings by RPI in May 2000. Frequency from 10 to 100 kHz is displayed versus echo travel time in ms. (d) Plot of the low-altitude portion of the IMAGE polar orbit for the case of Figure 4a. The approximate location of IMAGE is indicated by a red dot, as are the locations for cases in Figures 4b and 4c. Dipole field lines at $L = 4$ are shown as a reference. The magnetic local times for the cases in Figures 4a, 4b, and 4c were 22.61, 10.49, and 11.31, respectively.

indicator of the plasmasphere boundary, not specific to any of the cases illustrated. The values of local f_{ce} as obtained from a geomagnetic field model (IGRF) are 730, 321, and 341 kHz for the cases a, b, and c, respectively; the values of local f_{pe} as estimated from the matching of observed dispersion with that obtained from ray tracing calculations (as discussed in section 4.1) are 359, 180, 252 kHz for the cases a, b, and c, respectively. The occurrence of whistler mode propagation is indicated by echo frequencies below the local f_{ce} and f_{pe}. As expected, the echoes formed a continuous curve in $f - t$ space and showed an increase in delay with decreasing frequency.

[35] As in the cases of Figures 2 and 3, we believe that the discrete echoes shown here are the result of signal reflections from the bottom side of the ionosphere. The echo frequencies are above the maximum lower hybrid frequency in the ionosphere, ≈12 kHz; the average group velocity for propagation from IMAGE to the bottomside ionosphere and back is about $c/3$ or lower, consistent with slow whistler mode propagation. The altitudes of observations were ≈1500 km for Figure 4a and ≈4000 km for Figures 4b and 4c, this difference being coarsely reflected in the differences in whistler mode round-trip travel time illustrated.

3.5. Diffuse Echoes in the Polar Region

[36] When sounding over the southern polar region, RPI has observed strong echoes with delays spread well beyond those observed in "discrete" whistler mode events such as those of Figures 2, 3, and 4. To illustrate this effect, we return to the time-delay-versus-frequency plasmagram display format, as in Figures 2a and 2b. Figures 5a–5c show examples of wide spreading in time delay of whistler mode echoes, called diffuse echoes, typically received outside the plasmapause at low altitudes over the polar region. Whistler mode echoes were accompanied by Z mode echoes in all three cases and by a free space R-X mode echo in Figure 5c. Figure 5d shows the approximate

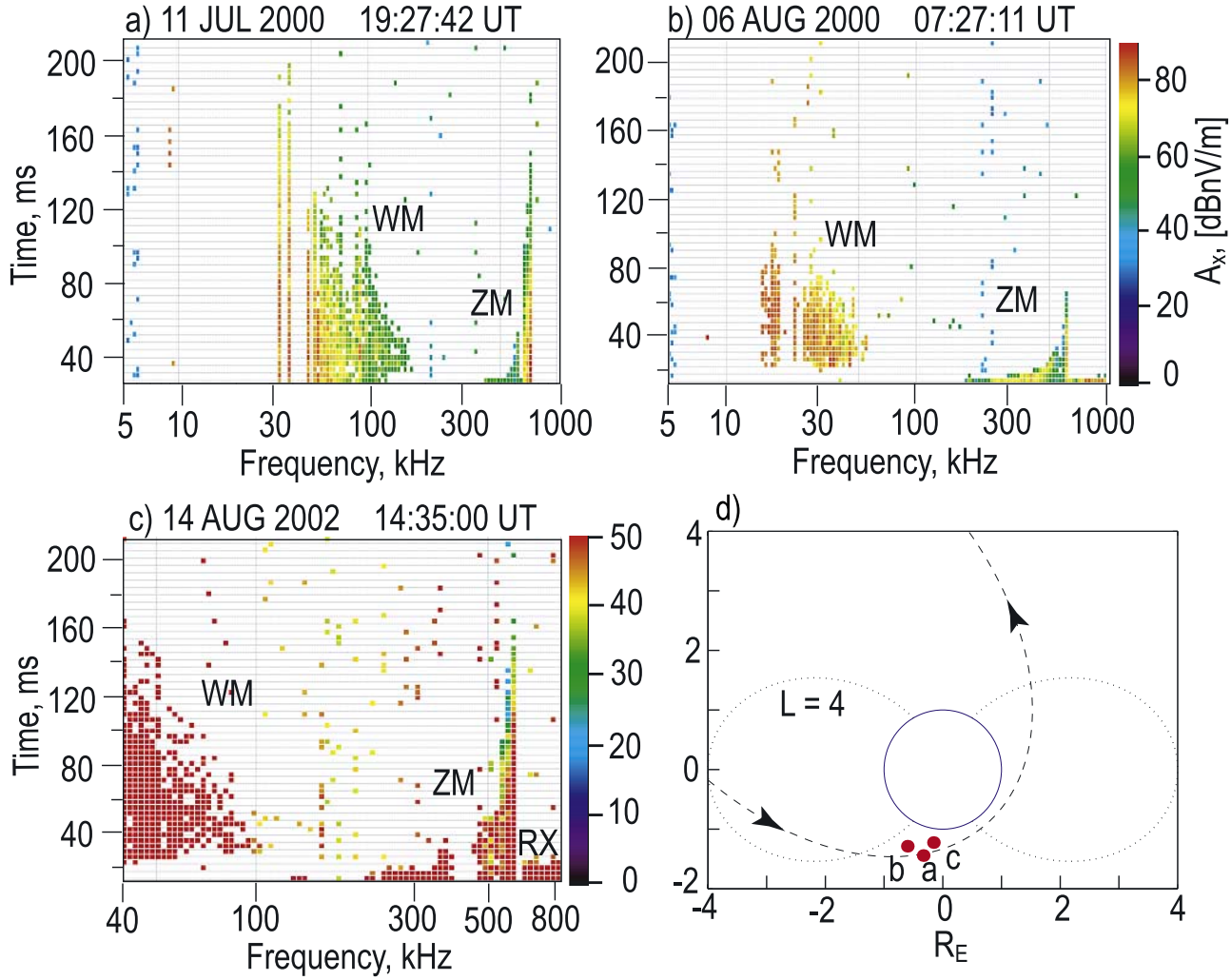

Figure 5. (a–c). Plasmagrams showing examples of wide spreading in time delay leading to diffuse whistler mode echoes received outside the plasmapause at low altitudes over the southern polar region. Whistler mode echoes were accompanied by Z mode echoes in all three cases and by a free space R-X mode echo in Figure 5c. (d) Plot of the low-altitude portion of the IMAGE polar orbit for the case of Figure 5a. The approximate location of IMAGE is indicated by a red dot, as are the locations for cases in Figures 5b and 5c. Dipole field lines at $L = 4$ are shown as a reference. The magnetic local times for the cases in Figures 5a, 5b, and 5c were 9.11, 3.37, and 9.22, respectively.

locations of IMAGE for these cases with respect to the low-altitude portion of the IMAGE polar orbit for the case of Figure 5a. In Figures 5a and 5b, two 3.2-ms pulses were transmitted at each of 178 frequencies logarithmically spaced over the frequency range 5–1000 kHz. For the case of Figure 5c, a single 3.2 ms pulse was transmitted at each of 78 frequencies logarithmically spaced over the range 40–800 kHz. In all cases, the amplitude is shown in dB(nV/m) as received on the long X antenna.

[37] In contrast to the discrete echo events of Figures 2, 3, and 4, in which time delay spreading at each frequency varied from ≈3 to ≈20 ms, in Figure 5a the echoes were spread over as much as 100 ms at frequencies between ≈50 kHz and ≈160 kHz, with the most pronounced spreading at the lower frequencies. In Figure 5a the minimum detectable time delay was ≈25 ms, and it is clear from Figure 5a that the minimum delay for the diffuse echo was shorter than this. Z mode echoes are visible between ≈420 kHz and 727 kHz. Following the discussion earlier, we find from the Z mode echo characteristics $f_{ce} \sim 620$ kHz and $f_{pe} \sim 380$ kHz. Clearly, the whistler mode echo frequencies were below both f_{ce} and f_{pe}, as expected.

[38] The characteristics of diffuse echoes as well as Z mode echoes in Figures 5b and 5c are similar to those seen in Figure 5a. In Figure 5b, the echoes are spread over 85 ms at frequencies between 15 and 55 kHz, and in Figure 5c over 125 ms between 40 and 95 kHz. As in the case of Figure 5a, there was a trend toward wider time spread at the lower frequencies. In both of these cases, however, minimum time delays are resolved, thanks to a lower time delay limit of ≈13 ms on the record. From the measured Z mode characteristics, we found the values of local f_{ce} to be ∼575 and ∼565 kHz and the local f_{pe} to be ∼237 and ∼199 kHz for the cases b and c, respectively. It is clear that the whistler mode frequencies in both these cases were less than the local f_{ce} and f_{pe}.

[39] We suggest that the diffuse echoes (spreading effect) result from a process noted above, namely, scattering of transmitted electromagnetic whistler mode signals by small-scale (tens to hundreds of meters) field-aligned electron density irregularities. In a later section, we provide ray-tracing simulations in support of this interpretation.

3.6. Occurrence Patterns of Whistler Mode and Accompanying Z Mode Echoes

[40] We conducted surveys of RPI plasmagrams for periods ranging from 10 days to several months in the years 2000, 2001, and 2002. The survey times in 2000 and 2002 corresponded mostly to winter conditions over the southern polar region; in 2001 they corresponded to summer and fall. Each survey period involved several hundred intervals of RPI sounding in the low-altitude region of the orbit where whistler mode echoes might be expected to occur. The results on occurrence varied depending upon the type of sounding program in use, subjective criteria involved in pattern recognition, and factors such as the degree of interference from natural whistler mode auroral noise.

[41] In general, discrete and diffuse echoes were observed at altitudes lower than ≈5000 km and at magnetic latitudes above 30°–40°. Most diffuse echoes were found in the region poleward of the plasmapause, while discrete echoes were detected over a wide range of latitudes but were most common within the plasmasphere. Discrete and diffuse echoes were usually not seen on the same plasmagram. As discussed in the next section, this difference may be related to their different reflection mechanisms.

[42] As a fraction of all soundings below ≈5000 km, and hence at altitudes where whistler mode echoes might be expected, we found that either discrete or diffuse whistler mode echoes were clearly identifiable on ≈20%. When observed, such echoes tended to appear on more than one sounding, which were typically spaced by ≈1000 km along the same orbit. Overall, we conclude that one or more discrete or diffuse whistler mode echoes were detectable on at least half of all IMAGE orbits on which single 3.2-ms pulses were transmitted at the lower altitudes.

[43] Diffuse Z mode echoes were essentially omnipresent during soundings with 3.2-ms pulses in polar regions where $f_{pe}/f_{ce} < 1$, appearing on 90% of the plasmagrams containing whistler mode echoes and also on 90% of those on which such echoes were not evident.

[44] The observations of echoes also depended on the kind of processing used to detect them. Most of the statistics provided above relate to whistler and Z mode echoes observed when a single 3.2-ms pulse was transmitted at each frequency. The statistics for echoes resulting from a transmission program that involved coherent integration (see section 3.4) were different. For this program, out of 292 transmissions over the region where we expect to see whistler mode echoes, discrete echoes were detected 24 times, that is, during about 8% of the transmissions. Only one case of a diffuse whistler mode echo—a weak echo—was detected (along with a simultaneous discrete echo). In only 4 to 8 of the cases were these discrete whistler mode echoes accompanied by Z mode echoes, giving a ≈15–30% occurrence rate for this association compared to 90% for discrete cases obtained from the transmission of single 3.2 ms pulses. On those orbits on which no whistler mode echoes were detected, diffuse Z mode echoes were found during only ≈25% of the transmissions. This dependence of occurrence rates for whistler and Z mode echoes on the type of transmission format and processing is discussed in the next section.

[45] Discrete echoes appeared under a wide range of geomagnetic conditions. For example, on 31 March 2001, following a Kp of 9, whistler-like forms were found on five of six successive 180–245 kHz plasmagrams. During the relatively calm day of 3 July 2001, with Kp in the 1–2 range, whistler-like forms appeared on five soundings distributed from the central polar cap to the outer low-altitude plasmasphere, as in the case of Figure 3 for 12 July 2001. On average, during a multiweek period, the character of the whistler mode echoes in the polar regions changed from being more discrete to more diffuse as the level of magnetic disturbance increased.

4. Ray-Tracing Interpretation of Observed Whistler and Accompanying Z Mode Echoes

[46] In this section, we show, by ray-tracing analysis, that the observed features of a discrete echo are consistent with the reflection of RPI signals from a sharp Earth-ionosphere boundary at ≈100 km altitude. We also show that the properties of diffuse echoes are consistent with the scattering of RPI signals from small-scale field-aligned irregularities located at a distance intermediate between IMAGE and the bottom side of the ionosphere. Ray tracing also indicates that diffuse Z mode echoes are the result of scattering from field-aligned irregularities.

[47] The Stanford 2-D ray tracing employs a dipole field model, a diffusive equilibrium model for density along field lines within the plasmasphere, and an (R^{-n}) density falloff outside the plasmasphere [*Inan and Bell*, 1977]. We assume an $R^{-4.5}$ density variation outside the plasmasphere so as to closely match a "collisionless" model (R^{-4}) at middle invariant latitudes [e.g., *Eviatar et al.*, 1964; *Angerami and Thomas*, 1964; *Angerami*, 1966] as well as an R^{-5} empirical model at high latitudes [e.g., *Persoon*, 1988]. Since our ray-tracing simulations are at relatively low altitude, our results are not sensitive to the value of the exponent in the R^{-n} model.

[48] In the ray tracing, a reference electron density $n_{e,ref}$ is assigned at a given altitude and latitude; the magnetospheric density model is then scaled accordingly. The reference density is initially selected on the basis of available measurements or models and is then adjusted to obtain consistency between the ray tracing and observed wave properties such as dispersion. Overall, our density model and the reference densities considered are consistent with previous measurements [*Persoon et al.*, 1983, 1988; *Persoon*, 1988; *Kletzing et al.*, 1998; *Nsumei et al.*, 2003] in the region near IMAGE locations on the days considered.

[49] In the ray-tracing program, reflections at the Earth-ionosphere boundary are modeled as specular reflections at a specified altitude, typically 100 km. This assumed reflection is an approximation to the more complicated case of a full-wave treatment, which is essential for a complete analysis. The ray-tracing program also neglects *D* region absorption, which is important in daytime and increases with frequency [*Helliwell*, 1965].

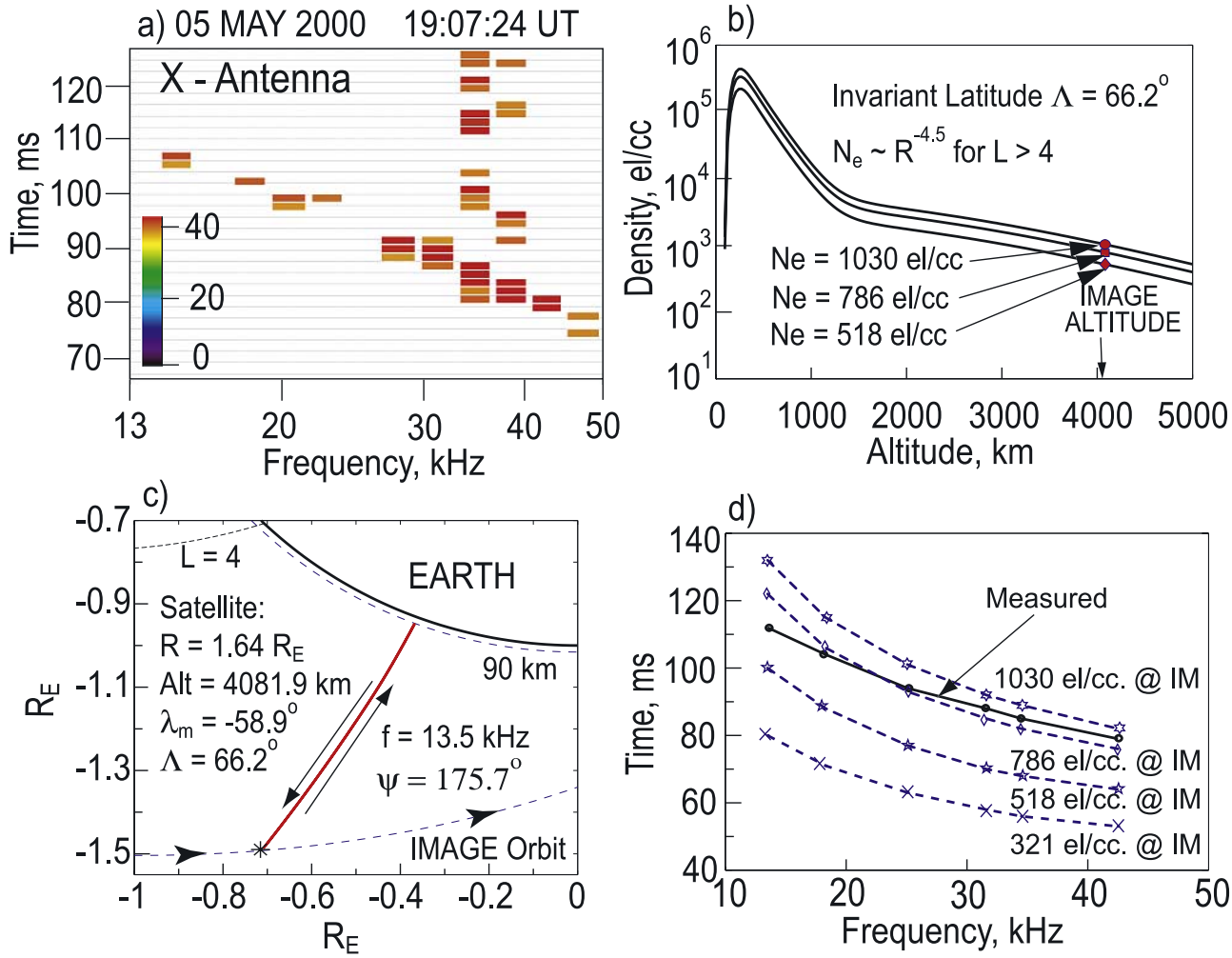

Figure 6. Example of a ray-tracing analysis performed to explain the propagation of an RPI signal that led to a discrete whistler mode echo. (a) Portion of the plasmagram of Figure 4c in $t - f$ representation showing the dispersion of the discrete echo detected on 5 May 2000. (b) Ray-tracing density model used. A diffusive equilibrium model is used for the plasmasphere ($L < 4$) and an $R^{-4.5}$ dependence outside the plasmapause for various $n_{e,ref}$ values near the satellite location. (c) Ray-tracing example showing propagation of a nonducted ray to the bottom of the ionosphere and back to the IMAGE satellite. (d) Results of ray-tracing analysis showing calculated and measured time delays for various local densities.

[50] In general, waves injected from IMAGE may propagate in either a nonducted or ducted mode to the reflecting altitude and then back to the satellite. The ray-tracing program permits simulation of both types of propagation. In the nonducted case, a plane wave tends to propagate with its wave normal within the whistler mode resonance cone $\theta_r \sim \cos^{-1}(f/f_{ce})$ but at some (usually large) angle with respect to **B**. The ray tends to be directed within a cone of angles around **B**, but the ray path is not constrained to follow a particular field line. In the ducted case, assumed to be associated with field-aligned columns of enhanced ionization, the ray paths remain closely aligned with the geomagnetic field [e.g., *Helliwell*, 1965; *Sonwalkar*, 1999], but the wave normal angles are not as tightly constrained as in the case of hemisphere-to-hemisphere propagation.

4.1. Discrete Whistler Mode Echo Interpretation

[51] Figure 6 shows how discrete echoes observed on 5 May 2000 (case shown in $f - t$ coordinates in Figure 4c) may be explained as the result of reflections from the Earth-ionosphere boundary. Figure 6a is a $t - f$ representation of a portion of the $f - t$ representation used in Figure 4c to illustrate a discrete echo. The density model used for ray-tracing calculations assumed the plasmapause to be at $L = 4$ (invariant latitude $\Lambda = 60°$). Figure 6b displays electron density ($n_e \sim R^{-4.5}$) along the dipole magnetic field ($\Lambda = 66.2°$) passing through the satellite for the various density profiles used in the ray-tracing calculations, referenced to the density at the satellite altitude. Rays are launched at various initial wave normal angles and allowed to reflect at the Earth-ionosphere boundary before returning to the satellite altitude of ≈4000 km. The returning ray closest to the satellite location is assumed to simulate the propagation of the observed echo (two closely spaced rays arriving on two sides of the satellite are used to estimate this ray). Figure 6c shows an example of nonducted ray propagation from the satellite to the Earth-ionosphere boundary and back to the satellite, while Figure 6d shows time delay as a

function of frequency predicted for the various density models. Time delays for the downward and upward propagation segments were found to be roughly the same. The field-line electron density model with 786 el cm^{-3} at the satellite location provided a close fit to the measured delays. Unfortunately for this case—unlike the one discussed in section 4.2.2—it was not possible to estimate the local electron density from resonances or cutoffs on nearby plasmagrams, or from features on the dynamic spectrum, to compare with the n_e = 786 el cm^{-3} that gave the best ray-tracing results.

[52] In addition to time delays, the ray-tracing program calculates propagation parameters such as wave normal angle and refractive index as well as various medium parameters along the ray path. We found that the ray propagation paths at the observed whistler frequencies (from 13.5 kHz to 42.5 kHz) were all very close to the field line through the satellite, and that they shared a number of features. At all frequencies, the initial wave normals for downgoing rays were within 1° of 175° (the magnetic field is assumed to be directed upward) and the wave normal angles of the returning rays were within 0.1° of 1.77°. The principal variation with frequency was in the value of the refractive index and the time delay. The refractive index, on the average, was ≈3.8 for 13.5 kHz and ≈2.4 for 42.5 kHz. The maximum f_{lh} along the path was ≈9.5 kHz, implying that MR reflection was not possible for these rays. We conclude that reflection from the Earth-ionosphere boundary is a plausible mechanism for echo generation in this case.

[53] A similar analysis was carried out for 9 cases of discrete echoes from an April–August 2000 period. In seven of the cases we could match the observed dispersion (time delay as a function of frequency) with that calculated from ray tracing assuming nonducted propagation. In two cases it was necessary to include ducts in the magnetospheric density model in order to match the observed and calculated dispersions. In one case with a duct at L = 3.1 the duct half width and density enhancement required were 0.1L and 70%, respectively, and in the other case with a duct at L = 4.9 they were 0.1L and 60%, respectively.

[54] Previous studies of the propagation of whistler mode waves from ground sources to satellites suggest that such waves commonly propagate on multiple closely spaced paths as they penetrate the ionosphere, due to the presence of field-aligned density irregularities of 1–10 km spatial scale length [*Sonwalkar et al.*, 1984]. Such structure should also affect whistler mode echoes from RPI and may help to explain the amount of time spreading (≈20 ms) seen in cases such as those of Figures 3 and 4.

4.2. Diffuse Whistler Mode Echo Interpretation

4.2.1. Conceptual Approach

[55] Diffuse whistler mode echoes exhibit substantial spreading in time delay and in many cases a relatively short minimum time delay at each frequency. To explain the time delay spreading, we consider the subset of injected waves with wave normals from 0° to within ≈2° of the resonance cone. These waves propagate downward with group velocities not far below a maximum value associated with propagation exactly along **B** (this is a reasonable assumption because for $f \ll f_{ce}$, most of the radiation is expected to be confined to a lobe in the direction of the magnetic field [*Sonwalkar et al.*, 2001]). At some altitude, or range of altitudes, the waves encounter field-aligned irregularities that are spread in latitude (and longitude). The nature of the irregularities is such that when incident upon them, whistler mode waves are scattered back (through a two-stage process mentioned in section 3.1) with wave normals spread over a large range of angles, including those within ≈2° of θ_{res}. For these latter waves the refractive index increases rapidly as θ approaches θ_{res}, so that they reach the satellite with widely spread time delays.

[56] As a consequence of this situation, waves that undergo scattering into angles that are not within ≈2° of θ_{res} propagate comparatively rapidly in both directions and thus can have reflection points relatively far from the satellite. Meanwhile, the waves most strongly scattered, with wave normals closely approaching θ_{res} and hence propagating very slowly, must have reflection points relatively near the satellite. The locations of the most distant possible and closest possible reflection points in a given case may be estimated by attributing the shortest observed echo delays to injected waves propagating in both directions along **B** and the longest observed delays to returning echoes with wave normal angles as close to θ_{res} as is possible without encountering limitations imposed by finite plasma temperature.

[57] Cold plasma theory predicts an open refractive index surface for $f > f_{lh}$, and in principle $\mu \rightarrow \infty$ as $\theta \rightarrow \theta_{res}$ and $v_{gr} \rightarrow 0$ as $\theta \rightarrow \theta_{res}$. An estimate of minimum scatterer distance can thus be made based upon considerations of how large the refractive index can reasonably be.

[58] Landau damping of the scattered waves can occur when the parallel phase velocity $\omega/k_{\|} \sim V^e_{\|}$, where $k_{\|}$ and $V^e_{\|}$ are the wave normal vector and thermal electron velocity components along **B**, respectively. This places an upper limit on possible values of μ in terms of electron temperature: $\mu(\theta \sim \theta_{res}) \leq \sqrt{m_e c^2 \sec^2\theta_{res}/k_B T_e}$, where m_e and T_e are the electron mass and temperature and k_B and c are the Boltzman constant and velocity of light in vacuum [*Sonwalkar et al.*, 1995].

4.2.2. Application to the Case of 6 August 2000

[59] Ray tracing analysis along the lines just described has been applied to the case of 6 August 2000 in Figure 5b (plasmagram repeated in Figure 7a) and is summarized in Figure 7. In the ray tracing example of Figure 7b, ray paths from a single IMAGE location are for simplicity used to illustrate both whistler and Z mode echo activity; between the time of the first whistler mode echo at 15.6 kHz and the last Z mode echo at 622 kHz, the satellite moved from R = 1.39 R_E to R = 1.34 R_E.

[60] The ray-tracing density model used is essentially the same as the one discussed earlier, but in this case it was possible to estimate the local electron density and its variations along the orbit of IMAGE as the echoes were received. These estimates were based upon the measured upper hybrid $f_{uh} \approx$ 622 kHz and the estimated $f_{ce} \approx$ 599 kHz at the location where the 622 kHz signal was transmitted (1.34 R_E and $\lambda_m = -72.66°$), which imply that the local f_{pe} was ≈168 kHz and $n_e \approx$ 350 el cm^{-3}. These became the reference values for the purpose of extrapolation to other locations. (In general, information on the local f_{ce} was obtained either from the T96

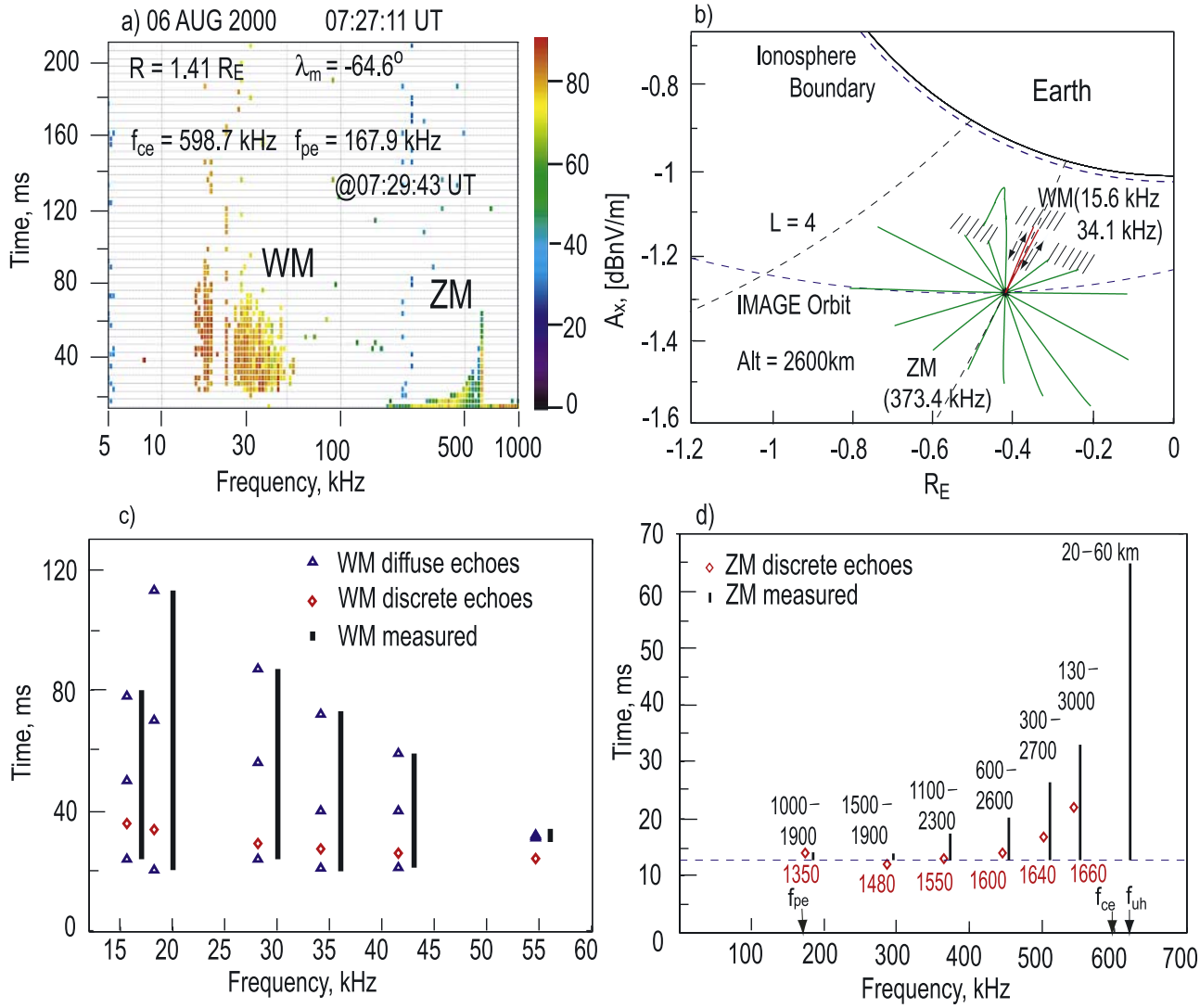

Figure 7. Example of ray-tracing analysis performed to explain propagation on 6 August 2000 of RPI signals that led to diffuse whistler mode (WM) and Z mode (ZM) echoes. (a) Plasmagram from Figure 5b showing diffuse whistler and Z mode echoes on this day. (b) Ray-tracing example showing propagation of nonducted whistler mode (red) and Z mode (green) rays to field-aligned irregularities and back to the IMAGE satellite. (c) Results of ray-tracing analysis showing calculated time delays for RPI signals scattered back from field-aligned irregularities at various wave normal angles (blue triangles) and those reflected from the bottom of the ionosphere (red diamonds). Measured time delays, which are spread over a range for each frequency, are shown by black vertical bars. (d) Results of ray tracing for Z mode wave propagation showing time delays (red diamonds) assuming that Z mode waves propagated along the geomagnetic field line and reflected at $f = f_Z$ at a certain distance (numbers in red below the diamonds) from the satellite. Black bars show the measured time delays, and the numbers above them represent distances that Z mode waves should travel in various directions in order to produce time delays equal to the measured ones.

magnetic field model [*Tsyganenko and Stern*, 1996] or directly from sounder-stimulated harmonics of the electron gyrofrequency).

[61] Could the echoes in Figure 7a be explained in terms of reflections at the Earth-ionosphere boundary (similar to those shown in Figure 6c)? Red diamonds in Figure 7c show for a few selected frequencies (15.6, 18.2, 28.1, 34.1, 41.5, 54.6 kHz) the delays that would be expected, based upon a satellite location at 1.38 R_E, midway through the diffuse whistler mode echo activity. The black vertical bars show the entire range of measured time delays obtained at the same frequencies (see Figure 7a). It is clear that even with allowances for spreading of up to 20 ms, as in Figure 3a, reflections from the Earth-ionosphere boundary cannot explain the longer time delays or the overall spread in delays. Such echoes may well have been present, but were masked on the record by the earliest-arriving diffuse echoes. Furthermore, the maximum f_{lh} over the ray path was less than 6.3 kHz, indicating that the diffuse echoes could not have been produced by magnetospheric reflections at f_{lh}.

We thus conclude that the observed echoes are attributable to scattering from irregularities.

[62] The most distant possible location of irregularities, needed to explain the shortest time delays of ≈20–24 ms due to the most rapidly propagating waves (i.e., those not propagating near the θ_{res} direction), was found to be ≈1.08 R_E or ≈500 km altitude. Ray tracings performed at all wave normal angles indicated that down going rays could reach that approximate altitude over a range of latitudes from ≈−68° to −74°.

[63] The closest possible location of irregularities was found to be ≈35 km from IMAGE, based upon the measured maximum time delay of 113 ms at 18.2 kHz and the slowly propagating waves at wave normal angles near θ_{res}. Assuming an electron temperature of roughly 1 eV [*Kletzing et al.*, 1998], we find that $\mu \leq 3000-10000$ for $f \sim$ 15–40 kHz, with lower values for the higher frequencies. These limiting values for μ impose corresponding limits on the lowest possible group velocities, from 300–340 km/s for $f \sim$ 15–40 kHz.

[64] The nearest and most distant possible inferred locations of scatterers are not the most probable, involving as both do very restricted conditions on scattering (return propagation along **B** for the most distant, maximum scattering for the nearest). Thus as one scattering scenario among the many that could explain the observed delays we assumed the irregularity location to be at ≈1.2 R_E (≈1270 km altitude), intermediate with respect to the two extreme locations possible. At this location $f_{pe} \approx$ 246 kHz (n_e was ≈750 el cm^{-3}), $f_{ce} \approx$ 820 kHz, and $f_{lh} \approx$ 3.7 kHz. Ray tracings from the satellite, performed at all wave normal angles, then indicated that downgoing rays could reach altitudes slightly above 1270 km over a range of latitudes from −67.7° to −71.8°. Short black lines shown in Figure 7b represent irregularities at such locations.

[65] At each of the six selected frequencies we carried out upward ray tracings from points throughout the −67.7° to −71.8° latitude range, seeking wave normal angles up to the resonance cone angle such that the rays would reach the satellite and the total round-trip time would agree with the measured minimum, intermediate and maximum delays (the resonance cone angle varied between ≈86.3° at 15.6 kHz and ≈76.6 at 54.6 kHz). Rays from only that portion of the −67.7° to −71.8° range within ≈±0.8° in latitude around $\lambda_m \approx -68.5°$ were able to reach the satellite. At 1.2 R_E, the latitude of the geomagnetic field line passing through IMAGE is −69.9°, implying that the scatterers were located close to the IMAGE field line with a spread of ∼500 km or more in the cross-**B** direction. In this calculation we have taken into account the satellite motion as the sounder frequency was stepped through the range of whistler mode echo frequencies.

[66] Figure 7b shows two examples of rays (in red) at 15.6 and 34.1 kHz that returned to the satellite after scattering. In Figure 7c the round-trip delays, calculated for signal paths corresponding to the shortest, longest, and an intermediate-value delay at each frequency, are shown as blue triangles. In each case we assumed that the downgoing waves had wave normal angles which were anywhere from parallel to **B** to within ≈2° of the resonance cone. These downgoing waves contributed about 5–8 ms of time delay. Most of the total time delay of an echo was contributed by upgoing scattered signals at wave normals close to the resonance cone angle. To explain the minimum round-trip delay of ≈20–24 ms, the initial wave normal angles required of the scattered upgoing waves were within a degree of the resonance cone angle, and the refractive indices ranged from 15 to 60, with the larger values for the lower frequencies. Corresponding numbers for the intermediate time delays (30–70 ms) were wave normal angles within ≈0.1° of the resonance cone angle and refractive indices between 40 to 200. For the longest time delays (60–110 ms) and the 15.6–41.5 kHz echoes, the wave normals were within ≈0.005–0.05° of the resonance cone angle, and the refractive indices were between 60 to 300. To explain the ≈30 ms delay of 54.6 kHz echoes, the initial wave normal angle was within 0.5° of the resonance cone and the refractive index was ≈20. The general tendency of the echoes to have a larger time delay spread at the lower frequencies is probably related to the group velocity being lower at the lower frequencies.

[67] The refractive indices and wave normal angles obtained from the above calculations imply that the irregularities needed to scatter the incident whistler mode waves had spatial scale lengths distributed over 50 m to 500 m. Field-aligned irregularities with scale sizes ranging from a few meters to kilometers and with density fluctuations varying from a few percent at smaller scale sizes (≈10 m) to as much as 100% or more at larger ones (1–10 km) are commonly present in the midlatitude and high-latitude magnetosphere up to altitudes of several thousand kilometers [e.g., *Fejer and Kelley*, 1980; *Bell and Ngo*, 1988, and references therein; *Persoon et al.*, 1983, 1988; *Sonwalkar*, 1995]. In the past, scattering from such irregularities has been proposed to explain the spectral broadening of ground transmitter signals observed on the ISEE 1, DE 1, Aureol-3, and ISIS-2 satellites [*Bell and Ngo*, 1988; *Tanaka et al.*, 1987; *Ohnami et al.*, 1993]. We believe that diffuse echoes and spectral broadening are both manifestations of the scattering of whistler mode waves into quasi-electrostatic LH waves by field-aligned irregularities. We further note that the region where spectral broadening phenomena were detected [*Bell and Ngo*, 1988; *Sonwalkar*, 1995] includes the regions where diffuse echoes are detected.

[68] On the basis of our inspection of other cases, we believe that the scenario proposed here for the data of 6 August 2000 case can also explain other cases of diffuse echoes.

4.3. Diffuse Z Mode Echo Interpretation

[69] As mentioned earlier, whistler mode echoes, both the discrete and diffuse type, are almost always accompanied by Z mode echoes. In high-latitude regions where $f_{pe}/f_{ce} < 1$, the Z mode echoes are usually diffuse in character and span a wide band of frequencies, consistent with Z mode propagation. The time delay for these echoes increases with frequency, as seen in Figures 2 and 5. A general description of these diffuse Z mode echoes and some comments on their interpretation have been presented by *Carpenter et al.* [2003]. Here we provide a ray-tracing interpretation of their generation mechanism. In agreement with *Carpenter et al.* [2003], we believe that these diffuse Z mode echoes are in part the result of scattering by field-aligned irregularities in the vicinity of the satellite. We use ray-tracing for the

Figure 5b case of 6 August 2000, repeated in Figure 7a, to test this hypothesis.

[70] We envision that Z mode echoes can occur in two different ways: (1) At any given frequency f below local f_{ce} the Z mode waves may propagate Earthward in the approximate direction of the geomagnetic field and reflect at altitudes where $f = f_Z$, the low-frequency cutoff of Z mode propagation, and then return to the satellite, again in the field-line direction. This kind of propagation scenario can be operative for echoes below f_{ce} only, since above f_{ce} and below f_{uh} propagation parallel to the geomagnetic field is not allowed (see Figure 1b). The scenario is believed to explain discrete Z mode echoes trapped in Z mode "cavities" in the plasmasphere and plasmasphere boundary layer [*Carpenter et al.*, 2003]. (2) At any given frequency f below the local f_{ce}, waves spread out in all directions, as allowed by the closed refractive index surface at these frequencies. They encounter density irregularities that scatter the incident waves, some of which make it back to the satellite. For frequencies between f_{ce} and f_{uh}, Z mode propagation is allowed within a resonance cone that permits propagation in the direction roughly perpendicular to the geomagnetic field. These waves can also lead to echoes after scattering from density irregularities aligned with the field as has been well documented by ionospheric topside sounders [e.g., *Muldrew*, 1969; *James*, 1979]. Ray-tracing results discussed below suggest that the second mechanism is regularly operative during sounding at low and medium altitudes.

[71] Figure 7b shows examples of Z mode ray tracing at f = 373.4 kHz, above f_{pe} = 168 kHz, but below f_{ce} = 599 kHz. Rays injected at various wave normal angles covering the range 0°–180° are shown in green. In contrast to the whistler mode rays (red), the Z mode rays spread out in all directions, encountering electron density irregularities in the neighborhood of the satellite in directions not necessarily along the geomagnetic field. Ray tracings were carried out at seven frequencies: 184.3, 295.1, 373.4, 455.3, 511.1, 552.8, 620.0 kHz. The first six frequencies are above f_{pe} but below f_{ce} and the last one between f_{ce} and f_{uh}; they all propagated in the slow Z mode, that is, in the large-k region of Figure 1b where the refractive index of Z mode wave is larger than unity.

[72] The results of the ray-tracing simulations are shown in Figure 7d. Red diamonds show the calculated time delays at the lower six frequencies ($f < f_{ce}$), assuming that the rays propagated along the geomagnetic field line and reflected back at $f = f_Z$. The numbers in red show the distance of the reflection point from the satellite location for each frequency. For the highest frequency, parallel propagation is not allowed by the nature of the refractive index surface. The black bars show the entire range of measured time delays at each frequency, while the dashed horizontal line shows the minimum detectable delay time of 13 ms. It is clear that field-aligned propagation and reflections at $f = f_Z$, while not inconsistent with the data, and possibly masked by intense scattered signals, cannot explain the spread in observed delays.

[73] We next carried out ray-tracing simulations at each of the seven frequencies within a range of permissible wave normal angles that included 0°–90° for $f < f_{ce}$ and angles inside a resonance cone with axis perpendicular to the geomagnetic field for $f > f_{ce}$ (the resonance cone angle with respect to the geomagnetic field is ≈75° at 620.0 kHz, implying that the permissible wave normals lie in a narrow cone of ≈15° with axis perpendicular to **B**). We allowed each ray to propagate until the group delay time reached half of the maximum total delay time observed for echoes at the ray frequency. If we assumed that electron density irregularities at this location were capable of scattering Z mode waves back to IMAGE, we would obtain an echo with time delay equal to the observed maximum delay at that frequency. The pair of numbers listed above each of the black bars gives the range of distance in kilometers that Z mode waves at a given frequency must propagate in various directions before encountering plasma irregularities such that the observed maximum delay could be obtained. If a ray injected in a certain direction were to encounter irregularities before reaching this maximum distance, the corresponding echo delay would be less than the maximum observed at the ray frequency.

[74] Figure 7d shows that density irregularities located within ≈20–3000 km can lead to multiple echoes at each frequency with time delays that can match the observed ones. In terms of the efficiency of backscattering, we expect that the strongest echoes occur when the incident wave normal is perpendicular to **B**. Thus those waves propagating in directions generally transverse to **B** probably make the largest contribution to the observed echoes. The calculated refractive indices for Z mode waves at the point of scattering suggest that the irregularities involved had scale sizes ~70 m to 2 km.

[75] The overall nature of the observed time delays as a function of frequency is consistent with the theoretical properties of Z mode waves. For frequencies above f_{pe}, we have the slow Z mode with group velocity decreasing and time delay increasing with frequency for any given wave normal direction. Above f_{ce} and close to f_{uh} the Z mode becomes quasi-electrostatic and we expect much longer time delays. The frequently observed weakening of Z mode echoes at frequencies immediately above f_{ce} [*Carpenter et al.*, 2003] could be related to the change in the refractive index surface from a closed to an open topology as discussed by *Gurnett et al.* [1983], *LaBelle and Treumann* [2002] and *Carpenter et al.* [2003].

4.4. General Picture of Whistler and Z Mode Echoing Processes Indicated by the RPI Observations on IMAGE and Ray-Tracing Simulations

[76] Figure 8 schematically describes our overall views of whistler mode echoing processes and of Z mode echoing effects that occur in higher latitude regions where $f_{pe}/f_{ce} < 1$. A key feature of this picture follows from the nature of the refractive index surfaces for whistler and Z mode propagation. For $f > f_{lh}$, the whistler mode refractive index surface is open and, given that relatively short distances (<5000 km) are involved, the waves propagate with ray directions close to the geomagnetic field. Thus the echo generation process, both for discrete and diffuse echoes, is mostly determined by the plasma conditions along the field line passing through the satellite. On the other hand, the Z mode refractive index is closed up to f_{ce}, allowing propagation in all directions, and is then open with a resonance cone for $f_{ce} < f < f_{uh}$, allowing propagation mostly in the direction perpendicular to the geomag-

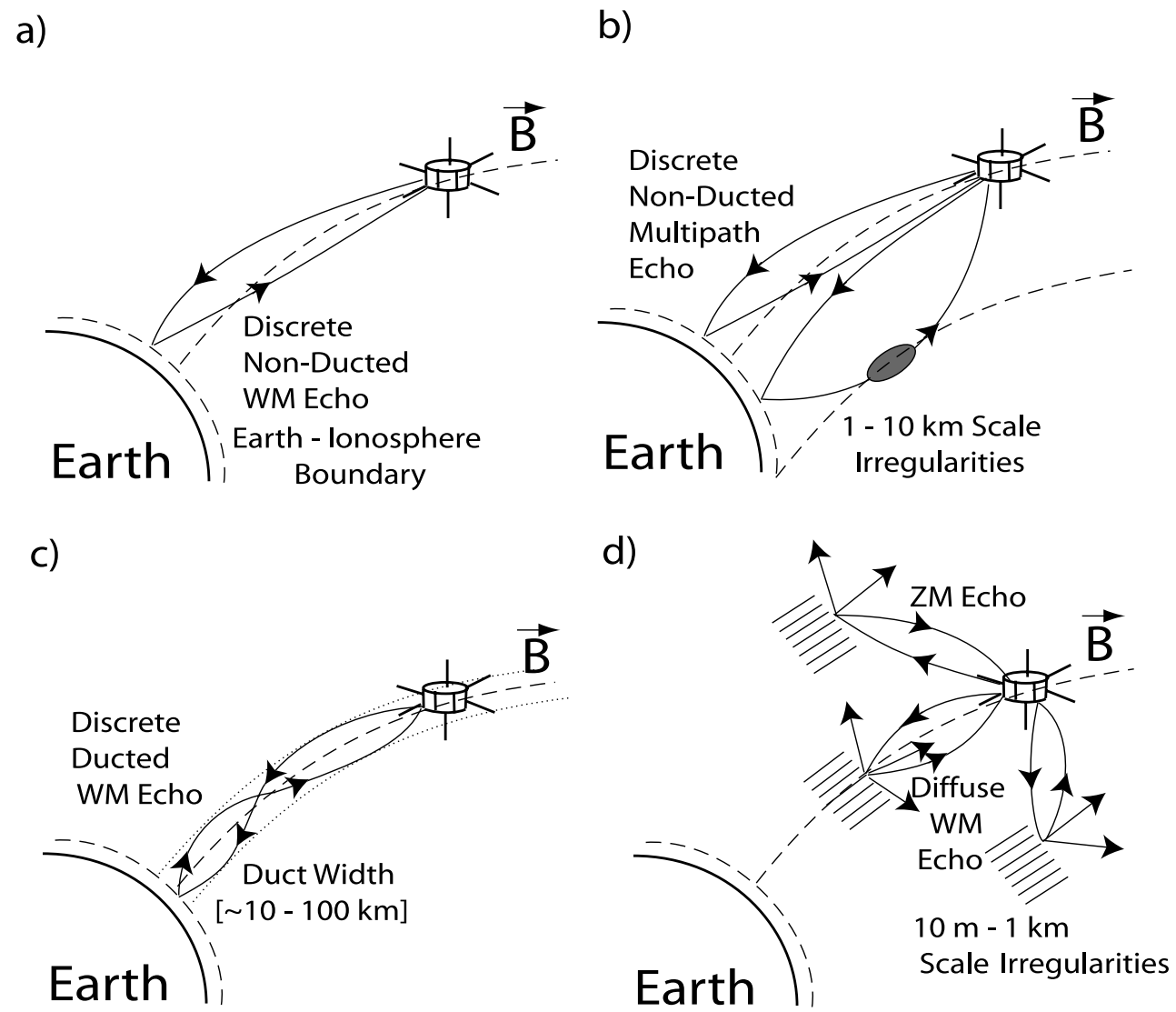

Figure 8. Schematic showing various propagation scenarios that may lead to whistler mode (WM) and Z mode (ZM) echoes observed on the IMAGE satellite. (a) Discrete whistler mode echoes with very little or no spreading ($\leq$5 ms) in time delays at each frequency, due to propagation of whistler mode signals in a magnetosphere that is relatively smooth in the neighborhood of the geomagnetic field line passing through the IMAGE location. (b) Discrete whistler mode echoes with medium time delay spreading ($\approx$10–20 ms) at each frequency, due to propagation along multiple paths to IMAGE in the presence of large-scale ($\approx$10 km) irregularities in the lower ionosphere. (c) Discrete whistler mode echoes, due to propagation of whistler mode signals inside field-aligned ducts. (d) Diffuse whistler mode echoes, due to scattering of whistler mode signals by small-scale (10 m to 1 km) irregularities located close to the geomagnetic field line passing through the IMAGE location. Z mode echoes are observed $\approx$90% of the time in high-latitude regions where $f_{pe}/f_{ce} < 1$, due to scattering from small-scale irregularities located close to the satellite but in any direction relative to that of the local geomagnetic field.

netic field. Thus for $f < f_{ce}$, Z mode echoes are indicative of plasma conditions near the satellite in all directions, and for $f > f_{ce}$, reflect conditions in the direction roughly perpendicular to the geomagnetic field. Another striking feature of this picture is the important role played in the echoing process by electron density irregularities with a wide range of scale sizes: tens of meters to hundreds of meters.

[77] Figure 8a depicts the situation for a discrete whistler mode echo with very little spreading in time delays at each frequency (e.g., Figure 2). These echoes probably result when the magnetosphere is fairly smoothly varying, at least close to the geomagnetic field lines passing through IMAGE. Thus the RPI signal can propagate down to the Earth-ionosphere boundary without major hindrance and return to the satellite. We expect a single echo at each frequency, leading to a discrete echo trace.

[78] Figure 8b depicts the situation for a discrete whistler mode echo with 20–30 ms spreading in time delays at each frequency (e.g., Figures 3 and 4). In these discrete echoes the spreading in time delays is attributed to multipath

propagation, involving refraction of RPI signals by large-scale (≈10 km) density irregularities following reflection from the Earth-ionosphere boundary. Field-aligned irregularities of ≈1–10 km or larger scale sizes located up to ≈500–1000 km altitude can lead to the observed multiple delays at each frequency in a way similar to that described for direct multipath propagation of ground transmitter signals observed on the ISEE-1 satellite [*Sonwalkar et al.*, 1984]. Because these ionospheric irregularities are present almost all the time [*Fejer and Kelley*, 1980], the discrete echoes almost always show some amount of spreading in time delay at each frequency.

[79] Figure 8c outlines the situation for ducted propagation of whistler mode echoes. One or more ducts, or field-aligned columns of enhanced or depressed ionization, should be present along or near the field lines passing through the satellite. Unlike ducts required for propagation of lightning whistlers, these ducts need not extend from hemisphere to hemisphere, and may have density enhancements of ∼50% or more. Such ducts are frequently present in the highly structured plasma at high latitude [*Persoon et al.*, 1983, 1988] and have been proposed to explain the propagation of impulsive auroral hiss to the ground [*Siren*, 1975; *Sonwalkar and Harikumar*, 2000]. Because of the relatively short propagation distances involved, waves with wave normal angles other than those very close to **B** may remain within the duct both before and after reflection. For ducted echoes to be seen on IMAGE, it is necessary that the duct extends to low enough altitudes such that whistler mode energy reflected at the Earth-ionosphere boundary is coupled back into the duct. It is conceivable that some of the reflected energy returns to the satellite along nonducted paths, as in sequences of ducted/nonducted signals reported in data from the DE-1 satellite [*Rastani et al.*, 1985].

[80] Figure 8d shows that for diffuse whistler mode echoes to be observed on IMAGE, it is necessary that there be field-aligned electron density irregularities on field lines close to the satellite.

[81] The Z mode echoes shown in Figure 8d occur where $f_{pe}/f_{ce} < 1$. They may accompany any one of the whistler echo forms of Figure 8, but most frequently appear with that of Figure 8d, which is regularly present in polar regions. We note that at high latitudes, the propagation of Z mode waves over long distances in all directions, including those perpendicular to the magnetic field, was indicated by observations of naturally occurring Z mode waves from the DE-1 satellite [*Gurnett et al.*, 1983].

[82] The general picture of whistler and Z mode echoes presented here provides a qualitative explanation of certain features of the occurrence patterns of these echoes discussed in the previous section.

[83] We do not see discrete and diffuse whistler mode echoes occurring together, because the former requires a smooth magnetospheric plasma near the geomagnetic field lines passing through the satellite, whereas the latter requires field-aligned irregularities present on the same field lines. Z mode echoes occur most frequently (≈90%), both in the presence and absence of whistler mode echoes, because the Z mode can propagate long distances in all directions, not only close to the field lines as in the case of the whistler mode. Thus there is a much larger probability of encountering plasma irregularities which may lead to Z mode echoes.

[84] The low occurrence rates of diffuse whistler mode and Z mode echoes during transmission programs involving coherent integration of 8 phase-coded 3.2-ms pulses may be explained in terms of scattering from small-scale (<1 km) irregularities. In a 2-s period during which the eight 3.2-ms chips are transmitted, the satellite travels about 16 km. Echoes coming from individual 3.2-ms chips are returning from regions with different characteristics as scatterers and may lack phase coherence. Such pulses when added may lead to cancellation such that weak integrated echoes that may have been generated may not be detectable over the background. In the case of discrete echoes that result from propagation of RPI signals in a relatively smooth magnetosphere, the coherent integration scheme has a better chance to achieve greater echo strengths.

5. Discussion

5.1. Ionospheric Reflections and Their Importance

[85] The rare whistler mode echoes in the 200–800 kHz range found at high latitudes in the ISIS program were interpreted in terms of ground reflections that followed a mode-coupling process in the lower ionosphere [*Muldrew*, 1969]. The regular observations by RPI of what are interpreted as ionospherically reflected whistler mode waves may be attributed to several factors, including greater radiation efficiency at whistler mode frequencies (the RPI transmitting antenna is a factor of ≈5–10 longer than the antennas used in the ISIS series) and the occasional use of coherent integration. In view of the efficiency with which RPI has produced whistler mode echoes at high polar latitudes, the possibility exists that the rare echoes found in the ISIS data were also the result of ionospheric reflection.

[86] There are persuasive theoretical arguments in support of a lower-ionosphere reflection process for whistler mode echoes. Upon reaching the altitudes of steep electron density gradients in the bottom side ionosphere at ≈90 km, nonducted whistler mode signals at frequencies above the maximum lower hybrid frequency in the ionosphere (≈10 kHz) are expected to have wave normal angles outside the narrow cone required for downward ionospheric penetration [*Helliwell*, 1965] and should thus be internally reflected. If the downgoing signals are initially confined to a duct, confinement is expected to end in the topside ionosphere as the normal ionospheric gradients become large enough to control further downward propagation [*Bernhardt and Park*, 1977]. Because there should be an angular spectrum of wave normal angles at the effective endpoint of the duct, a distribution of angles should then be present at the lower ionospheric boundary. Only a subset of these angles, however, may be close enough to the vertical to allow the associated waves to exit the ionosphere into the Earth-ionosphere waveguide.

[87] The geophysical importance of whistler mode reflections is suggested by observations showing that whistler mode waves propagating along a magnetospheric duct can spread widely as a result of ionospheric reflec-

tion, illuminating other ducts as well as nonducted paths [e.g., *Rastani et al.*, 1985; *Smith et al.*, 1985; *Carpenter and Orville*, 1989]. It will be recalled that in their classic paper on the limits of particle fluxes in the magnetosphere, *Kennel and Petschek* [1966] used an estimated whistler mode ionospheric reflection coefficient in discussing the role of whistler mode noise in maintaining an equilibrium state of energetic electron flux levels in the magnetosphere.

[88] Discrete RPI whistler mode echoes observed on IMAGE provide an opportunity to investigate the ionospheric reflection process as a function of frequency and geophysical parameters. During a single plasmagram recording of whistler mode echoes extending from ≈60 kHz to 300 kHz, as in Figure 2a, the satellite moves ≈200 km, with a corresponding change in the propagation path and region of reflection. From the observed distribution of echo properties with frequency, remote estimates of ionospheric and low-altitude plasmasphere ''smoothness'' may be obtained.

5.2. Electron Density Irregularities and Their Importance

[89] The auroral and polar ionospheres are highly structured regions containing electron density irregularities ranging in size from meters to hundreds of kilometers. Various processes are believed to cause the irregularities, including plasma instabilities, particle precipitation, and plasma drifts. Little detailed knowledge of polar region density and density structures is available, [e.g., *Sojka et al.*, 2000], although these phenomena are intimately tied to the physics of auroral acceleration processes, including polar ion outflow, auroral precipitation, visible and radar aurora, and substorm activity [e.g., *Kelley et al.*, 1990; *Schunk and Nagy*, 2000]. On the practical side, the irregularities are important because they contribute to the fading of high-frequency trans-ionospheric signals and to the degradation of ground-satellite communications. Forecasting and specification of the irregularities is a major component of space weather programs.

[90] In the past, in situ high-latitude electron density at low altitudes (≈2 R_E geocentric distance) has been determined primarily through either Langmuir probes [e.g., *Kletzing et al.*, 1998 and references therein] or topside sounding using the free space modes and plasma resonances [e.g., *Muldrew*, 1969; *Timleck and Nelms*, 1969; *Benson and Calvert*, 1979]. At higher altitudes (2–5 R_E geocentric distance), the upper cutoff of whistler mode radiation at f_{pe} was used to determine the electron density [e.g., *Persoon et al.*, 1983, 1988]. These studies have provided a picture of a high-latitude magnetosphere with highly variable electron densities and structures of various scales.

[91] Past work on whistler mode propagation [see *Smith*, 1960; *Helliwell*, 1965; *Bell et al.*, 1983; *Sonwalkar et al.*, 1984; *Bell and Ngo*, 1988; *Sonwalkar*, 1995, and references therein], as well the results on whistler mode echoes presented here, demonstrate that whistler mode propagation is profoundly affected by density irregularities of dimensions transverse to **B** ranging from meters to tens of kilometers and larger. The reason why the waves are strongly reflected, refracted, scattered, or guided by irregularities of such widely varying sizes is that, depending on the wave normal direction with respect to the geomagnetic field, the whistler mode refractive index can range over 3 orders of magnitude (≈1–1000).

[92] Three types of irregularities—ducts, large-scale features (1–10 km), and small-scale features (10 m to 1 km)—appear to influence whistler mode propagation. Each seems to be associated with certain characteristics of RPI whistler mode echoes.

[93] Ducts are field-aligned enhanced or depressed columns of ionization, typically ≈0.1L in width, that extend over long distances, often from one hemisphere to the other. It is generally accepted that ducts are responsible for the observation on the ground of lightning-generated whistlers [*Helliwell*, 1965] as well as impulsive auroral hiss [*Siren*, 1975; *Sonwalkar and Harikumar*, 2000] These waves could not otherwise have reached the ground because of the total internal reflection within the ionosphere expected for nonducted whistler mode waves propagating (typically) at large wave normal angles.

[94] Large-scale irregularities with spatial scale sizes of order 1–10 km can lead to multiple paths of propagation for waves injected from the ground or for those reflecting in the lower ionosphere at the Earth-ionosphere boundary or at an altitude where $f = f_{lh}$. This multipath propagation can affect the characteristics of the nonducted whistler mode waves as they subsequently move through a region of maximum wave-particle interactions along their path, thus reducing the effective length of that region [*Sonwalkar et al.*, 1984; *Bell*, 1984]. Multipath effects have also been proposed to be responsible for the generation of diffuse plasmaspheric hiss from discrete magnetospherically reflected whistlers [*Sonwalkar and Inan*, 1989; *Draganov et al.*, 1992]. Plasmaspheric hiss has long been considered to be an important factor in the maintenance of the stability of the radiation belt electrons [*Kennel and Petschek*, 1966; *Thorne et al.*, 1973].

[95] Scattering from small-scale ≈10–100 m irregularities has been considered to be responsible for the conversion of electromagnetic whistler mode waves into quasi-electrostatic lower hybrid waves. Both lightning-generated whistlers and auroral hiss have been proposed as sources for lower hybrid waves [*Bell and Ngo*, 1988, 1990; *Bell et al.*, 1991; *Sonwalkar and Harikumar*, 2000]. Such waves are important because they couple both to electrons and ions. It has been suggested that lower hybrid waves are the most efficient in heating suprathermal ions in the auroral region [*Lysak et al.*, 1980; *Chang and Coppi*, 1981; *Bell et al.*, 1993]. *Bell and Ngo* [1988] even suggest that, given that some process has led to the creation of a small-scale irregularity, it is possible that lower hybrid waves, generated by scattering of whistler mode waves, could work to maintain or enlarge the irregularity. Evidence has also been presented that ionospheric topside sounders can, under certain plasma conditions, either generate or enhance field-aligned irregularities [*Benson*, 1997].

5.3. Whistler Mode Diagnostics of Electron Density

[96] When IMAGE operates near or below 4000 km altitude, the whistler mode can supersede the free space modes for RPI sounding. At altitudes below ≈4000 km, the apparent ranges of the received O and X mode echoes approach the 0.3 R_E lower limit imposed by the minimum

3.2 ms RPI pulse length. The whistler mode is not restricted in this way, however, because of its low group velocity.

[97] Discrete whistler mode echoes can be used to investigate the electron density at altitudes up to about ≈5000 km along field lines near the plasmapause, in the auroral regions, and over the polar cap. These low-altitude regions, and their spatial n_e variations under various geophysical conditions, are poorly known.

[98] Diffuse whistler mode and Z mode echoes can be used to investigate electron density irregularities. The diffuse whistler mode and Z mode echoes provide complementary information: the whistler mode senses irregularities along the field line passing through the satellite while the Z mode senses those in the direction perpendicular to the local field line (echoes at $f_{ce} < f \leq f_{uh}$) as well as in all directions from the satellite (echoes at $f < f_{ce}$). The Z mode echoes also permit calculation of local electron density which can be used as a reference density in ray tracing.

[99] Following reception of a discrete whistler mode echo, ray tracing can be performed between IMAGE and the lower ionosphere, using an empirical model of the density variation with height. From the echo delay and dispersion, or variation in whistler mode travel time with frequency, it is possible to infer the scale factor of the density distribution along the field line as well as determine whether or not the whistler waves propagated in a ducted or nonducted mode. Changes in echo travel time from one sounding to the next and from sounding statistics will provide a basis for describing the density profiles in the low-altitude plasmasphere boundary layer. Echo amplitudes can be used in studies of ionospheric reflectivity over a wide range of L values and of path losses due to absorption and spreading.

[100] Additional constraints on ray tracings and thus on electron density models can be placed if, in addition to time delays, the wave normal angles of the received echoes are also used to match those from ray tracings. In principle, it is possible to determine the wave normal angle of the echoes from the echo amplitude and phase measured on three antennas as discussed in section 5.4 and also in *Sonwalkar et al.* [2001]. Echo time delay spreads of the order of 10–20 ms can be used to infer the presence of refracting order-of-10-km scale irregularities close to the ray paths returning from the Earth-ionosphere boundary.

[101] When time spreading of whistler mode waves becomes so great as to cause the electromagnetic aspects of the transmitted signals to be eclipsed by quasi-electrostatic echoes, as in the case of diffuse echoes, the ray-tracing analysis will change to focus on the properties of the field-aligned irregularities that cause them and on the mechanism(s) of generation of quasi-static whistler mode waves from incident electromagnetic whistler mode waves. Similar analyses may be performed on the diffuse Z mode to investigate the density irregularities occurring in the directions other than that along the field line passing through the satellite.

5.4. Some Remaining Issues: Measurement of Wave Normal Angle and Antenna Properties

[102] A number of specific questions involving RPI and the whistler mode remain to be addressed. These include the power radiated in the whistler mode, the effects of antenna orientation on transmitted and received signals, the wave normal angles of detected whistler mode echoes, the effects of the antenna coupler network on whistler mode transmissions, and the problem of detecting RPI signals at ground stations.

[103] It is possible to measure the wave normal direction of whistler mode echoes from the electric field magnitude and phase received on the three antennas by a method described by *Sonwalkar et al.* [2001]. This method assumes that the antenna effective length for each antenna is about the same as its physical length (or is proportional to its physical length). The method is based on the recognition that the wave normal angle of whistler mode signals is related to its polarization, which can be measured by the three RPI antennas. A method to simultaneously determine the wave normal direction and antenna effective length from the propagation of ground transmitter signals to a satellite was previously developed from Siple Station, Antarctica transmitter signals received on the DE-1 satellite [*Sonwalkar and Inan*, 1986]. This method can be modified and used to recalibrate the two long RPI antennas for their effective lengths (recalling that the antennas have suffered some damage) by measuring signals from ground transmitters on the three antennas. Because of the large change in refractive index from unity below the Earth-ionosphere boundary to ∼5–10 as the signal enters the lower ionosphere, such ground transmitter signals should have almost vertical wave normal angles close to the perigee (≈1200 km) of IMAGE. From this known wave normal angle, assuming whistler mode propagation, we can estimate the polarization ellipse for the electric field vector and thus the ratios of the electric fields along the three dipole antennas. Comparing these ratios with those of measured signals (voltages) on the three antennas, we can determine the effective lengths of the X and Y antennas with respect to that of the Z antenna (which is assumed to be known).

[104] There is a need for study of electric antenna operations in the magnetospheric plasma when kilovolt-level voltages are applied at whistler mode frequencies. At low frequencies (f < 300 kHz), the antenna capacitance is mainly due to the plasma sheath surrounding the antenna. This capacitance is a function of the antenna voltage and changes during an RF cycle. Thus the "impedance" of the antenna cannot be defined in the usual way. Under such conditions the antenna response is expected to be a nonlinear function of the applied voltage. Past works have obtained first-order estimates of electric dipole antenna impedance, efficiency, and radiation pattern using linear theory valid at low voltages [*Mlodnosky and Garriott*, 1963; *Wang*, 1970; *Wang and Bell*, 1972; *Inan et al.*, 1981]. One study has determined experimentally that the antenna effective length at VLF for a 200-m-long receiving dipole antenna on the DE-1 satellite [*Sonwalkar and Inan*, 1986] is the same as the physical length. However, there has been no experimental study of the radiation properties of a VLF antenna in space operating at high voltage.

[105] Special campaigns to study penetration of the ionosphere by whistler mode signals have been conducted, thus far without evidence of signal detection at

ground receivers. Various problems have limited the scope of these efforts, which are nevertheless ongoing.

6. Summary and Concluding Remarks

[106] Discrete whistler mode echoes of 3.2-ms and 25.6-ms sounding pulses have been observed on RPI during operations at altitudes generally less than ≈5000 km within the plasmasphere and over southern auroral and polar regions. These echoes are interpreted as reflections of RPI signals from the Earth-ionosphere boundary near 90 km altitude. On frequency-versus-time records, the echoes were whistler-like in form, exhibiting a falling-tone characteristic at the low-frequency end and confinement to frequencies below the lower of either the local electron plasma frequency f_{pe} or the electron gyrofrequency f_{ce}. During soundings with 3.2-ms pulses at or below ≈4000 km altitude within the plasmasphere where f_{pe} was larger than f_{ce}, there was evidence of a frequency of minimum delay or nose frequency, as cold plasma propagation theory would predict. Poleward of the plasmasphere, where f_{pe} was typically less than f_{ce}, whistler-like forms extending above 200 kHz were detected. In accordance with theory they exhibited upper limits near the local plasma frequency, and instead of a frequency of minimum delay, roughly constant delays with frequency above 200 kHz, the lower-frequency limit of many of the records. Discrete echoes were detected on ≈10–20% of the individual soundings, which were typically conducted at ≈1000 km intervals when IMAGE was at altitudes below 3000 km. When observed, the echoes tended to appear on more than one sounding. In one case that was illustrated, they appeared on 5 successive soundings extending from $L \approx 5.5$ to $L \approx 2.2$.

[107] Diffuse whistler mode echoes, showing a range of time delays at each frequency, have been observed on ≈10–20% of the individual soundings over the southern polar regions at altitudes typically less than 5000 km. Diffuse whistler mode echoes are interpreted as evidence of a previously observed process involving coupling between transmitted electromagnetic whistler mode signals and quasi-electrostatic modes excited at the boundaries of density irregularities, followed by an additional stage of reflection from small-scale n_e structures. Diffuse whistler mode echoes have been observed primarily from 3.2-ms pulses and only rarely on 25.6-ms pulses obtained from coherent integration.

[108] Diffuse Z mode echoes were found to be an essentially ubiquitous phenomenon wherever $f_{pe}/f_{ce} < 1$, having been detected during 90% of the soundings, both when whistler mode echoes were detected and when they were not. Diffuse Z mode echoes are interpreted as Z mode RPI signals scattering back from electron density irregularities present in the neighborhood of the satellite. As in the case of diffuse whistler mode echoes, the Z mode echo occurrence rate dropped by a factor of roughly 3 when 25.6-ms pulses employing coherent integration were used for sounding.

[109] Ray-tracing analysis provides natural explanations for many spectral features of the whistler and Z mode echoes as well as their occurrence patterns. A general picture of a highly structured high-latitude magnetosphere capable of reflecting, scattering, and guiding whistler and Z mode signals has emerged from this analysis.

[110] The ray-tracing analysis has also demonstrated that whistler and Z mode echoes can be used to remotely sense magnetospheric plasma at various scale lengths. The measured dispersion of discrete whistler mode echoes can be used to determine the plasma density along the field lines passing near the satellite as well as to identify ducted and nonducted modes of propagation. Diffuse whistler mode echo dispersion can be used to determine the presence and scale sizes of field-aligned irregularities along the field lines near the satellite. Z mode echoes provide information on local plasma density and on density irregularities in directions not accessible to whistler mode propagation. If the echoes are analyzed both within individual soundings and on successive soundings, it is possible to map changes as IMAGE moves from high-latitude polar and auroral regions through the plasmasphere boundary layer and into the main plasmasphere.

[111] Most of the whistler and Z mode activity reported here has been incidental to sounding experiments designed for the free space modes. The RPI results, however, demonstrate the high potential value to magnetospheric research of dedicated space-based whistler and Z mode wave injection experiments on future missions.

[112] **Acknowledgments.** The work at University of Massachusetts Lowell was supported by NASA under subcontracts to Southwest Research Institute and at QSS Group, Inc., under NASA contract NASW-97002. The work at Stanford University was supported by subcontract no. 03-08482 from the University of Massachusetts Lowell. The work at University of Alaska Fairbanks was supported by the Los Alamos National Laboratory under contracts 389AZ0017-97 and 65520-001-03-97, and by NASA under contract NNG04GI67G. We thank Jonathan Shih and Ankit Jain for assistance in the study of RPI whistler mode echo activity.

[113] Arthur Richmond thanks Masashi Hayakawa and Andy J. Smith for their assistance in evaluating this paper.

References

Angerami, J. J. (1966), A whistler study of the distribution of thermal electrons in the magnetosphere, Ph.D. dissertation, Radiosci. Lab., Stanford Univ., Stanford, Calif.

Angerami, J. J., and J. O. Thomas (1964), Studies of planetary atmosphere: 1. The distribution of electrons and ions in the Earth's exosphere, *J. Geophys. Res.*, *69*, 4537.

Bell, T. F. (1984), The nonlinear gyroresonance interaction between energetic electrons and coherent VLF waves propagating at an arbitrary angle with respect to the Earth's magnetic field, *J. Geophys. Res.*, *89*, 905.

Bell, T. F., and H. D. Ngo (1988), Electrostatic waves stimulated by coherent VLF signals propagating in and near the inner radiation belt, *J. Geophys. Res.*, *93*, 2599.

Bell, T. F., and H. D. Ngo (1990), Electrostatic lower hybrid waves excited by electromagnetic whistler-mode waves scattering from planar magnetic-field-aligned irregularities, *J. Geophys. Res.*, *95*, 149.

Bell, T. F., U. S. Inan, I. Kimura, H. Matsumoto, T. Mukai, and K. Hashimoto (1983), EXOS-B/Siple VLF wave-particle interaction experiments: 2. Transmitter signals and associated emissions, *J. Geophys. Res.*, *88*, 295.

Bell, T. F., U. S. Inan, V. S. Sonwalkar, and R. A. Helliwell (1991), DE-1 observations of lower hybrid waves excited by VLF whistler mode waves, *Geophys. Res. Lett.*, *18*, 393.

Bell, T. F., R. A. Helliwell, U. S. Inan, and D. S. Lauben (1993), The heating of suprathermal ions above thunderstorm cells, *Geophys. Res. Lett.*, *20*, 1991.

Benson, R. F. (1997), Evidence for the stimulation of field-aligned electron density irregularities on a short time scale by ionospheric topside sounders, *J. Atmos. Sol. Terr. Phys.*, *59*, 2281.

Benson, R. F., and W. Calvert (1979), ISIS 1 observations at the source of auroral kilometric radiation, *Geophys. Res. Lett.*, *6*, 479.

Benson, R. F., V. A. Osherovich, J. Fainberg, and B. W. Reinisch (2003), Classification of IMAGE/RPI-stimulated plasma resonances for the accurate determination of magnetospheric electron-density and magnetic field values, *J. Geophys. Res.*, *108*(A5), 1207, doi:10.1029/2002JA009589.

Bernhardt, P. A., and C. G. Park (1977), Protonospheric-ionospheric modeling of VLF ducts, *J. Geophys. Res.*, *82*, 5222.

Brice, N. M., and R. L. Smith (1965), Lower hybrid resonance emissions, *J. Geophys. Res.*, *70*, 71.

Budden, K. G. (1985), *The Propagation of Radio Waves: The Theory of Radio Waves of Low Power in the Ionosphere and Magnetosphere*, 669 pp., Cambridge Univ. Press, New York.

Burch, J. L. (2000), IMAGE mission overview, *Space Sci. Rev.*, *91*, 1.

Carpenter, D. L. (2004), Remote sensing the Earth's plasmasphere, *Radio Sci. Bull.*, *308*, 13.

Carpenter, D. L., and R. E. Orville (1989), The excitation of active whistler-mode signal paths in the magnetosphere by lightning: Two case studies, *J. Geophys. Res.*, *94*, 8886.

Carpenter, D. L., N. Dunckel, and J. F. Walkup (1964), A new very low frequency phenomenon: Whistlers trapped below the protonosphere, *J. Geophys. Res.*, *69*, 5009.

Carpenter, D. L., T. F. Bell, U. S. Inan, R. F. Benson, V. S. Sonwalkar, B. W. Reinisch, and D. L. Gallagher (2003), Z-mode sounding within propagation "cavities" and other inner magnetospheric regions by the RPI instrument on the IMAGE satellite, *J. Geophys. Res.*, *108*(A12), 1421, doi:10.1029/2003JA010025.

Chang, T., and B. Coppi (1981), Lower hybrid acceleration and ion evaluation in the supra-auroral region, *Geophys. Res. Lett.*, *8*, 1253.

Draganov, A. B., U. S. Inan, V. S. Sonwalkar, and T. F. Bell (1992), Magnetospherically reflected whistlers as a source of plasmaspheric hiss, *Geophys. Res. Lett.*, *19*, 233.

Dyson, P. L. (1978), Operational modes for a wave injection facility aboard spacelab and a sub-satellite, *NASA Tech. Memo. 79657*, 37 pp.

Eviatar, A., A. M. Lenchek, and S. F. Singer (1964), Distribution of density in an ion-exosphere of a nonrotating planet, *Phys. Fluids*, *7*, 1775.

Fejer, B. G., and M. C. Kelley (1980), Ionospheric irregularities, *Rev. Geophys.*, *18*, 401.

Fredricks, R. W., et al. (1978), Report of the AMPS wave injection facility definition team, *TRW 3247-6002-RU-01*, NASA Goddard Space Flight Cent., Greenbelt, Md.

Fung, S. F., R. F. Benson, D. L. Carpenter, J. L. Green, V. Jayanti, I. A. Galkin, and B. W. Reinisch (2003), Guided echoes in the magnetosphere: Observations by radio plasma imager on IMAGE, *Geophys. Res. Lett.*, *30*(11), 1589, doi:10.1029/2002GL016531.

Galkin, I., G. Khmyrov, A. Kozlov, B. Reinisch, X. Huang, and G. Sales (2001), New tools for analysis of space-borne sounding data, paper presented at 2001 USNC/URSI National Radio Science Meeting, Boston, Mass., 8–13 July .

Goertz, C. K., and R. J. Strangeway (1995), Plasma waves, in *Introduction to Space Physics*, edited by M. G. Kivelson and C. T. Russell, p. 356, Cambridge Univ. Press, New York.

Groves, K. M., M. C. Lee, and S. P. Kuo (1988), Spectral broadening of VLF radio signals traversing the ionosphere, *J. Geophys. Res.*, *93*, 14,683.

Gurnett, D. A., S. D. Shawhan, and R. R. Shaw (1983), Auroral hiss, Z-mode radiation, and auroral kilometric radiation in the polar magnetosphere: DE 1 observations, *J. Geophys. Res.*, *88*, 329.

Hayakawa, M. (1995), Whistlers, in *Handbook of Atmospheric Electrodynamics*, edited by H. Volland, p. 155, CRC Press, Boca Raton, Fla.

Helliwell, R. A. (1965), *Whistlers and Related Ionospheric Phenomena*, Stanford Press, Stanford, Calif.

Helliwell, R. A., and J. P. Katsufrakis (1974), VLF wave injection into the magnetosphere from Siple station, Antarctica, *J. Geophys. Res.*, *79*, 2511.

Helliwell, R. A., and J. P. Katsufrakis (1978), Controlled wave-particle interaction experiments, in *Upper Atmosphere Research in Antarctica*, *Antarct. Res. Ser.*, vol. 29, edited by L. J. Lanzerotti and C. G. Park, pp. 100–129, AGU, Washington, D. C.

Inan, U. S., and T. F. Bell (1977), The plasmapause as a VLF wave guide, *J. Geophys. Res.*, *82*, 2819.

Inan, U. S., T. F. Bell, R. A. Helliwell, and J. P. Katsufrakis (1981), A VLF transmitter on the space shuttle, *Adv. Space Res.*, *1*, 235.

James, H. G. (1979), Wave propagation experiments at medium frequencies between two ionospheric satellites: 3. Z-mode pulses, *J. Geophys. Res.*, *84*, 499.

Kelley, M. C., J. G. Ding, and R. H. Holzworth (1990), Intense ionospheric electric and magnetic field pulses generated by lightning, *Geophys. Res. Lett.*, *17*, 2221.

Kennel, C. F., and H. E. Petschek (1966), Limit on stably trapped particle fluxes, *J. Geophys. Res.*, *71*, 1.

Kletzing, C. A., F. S. Mozer, and R. B. Torbert (1998), Electron temperature and density at high latitude, *J. Geophys. Res.*, *103*, 14,837.

LaBelle, J., and R. A. Treumann (2002), Auroral radio emissions: Hisses, roars, and bursts, *Space Sci. Rev.*, *101*, 295.

Lysak, R. L., M. K. Hudson, and M. Temerin (1980), Ion heating by strong electrostatic ion cyclotron turbulence, *J. Geophys. Res.*, *85*, 678.

Mlodnosky, R. F., and O. K. Garriott (1963), The v.l.f. admittance of a dipole in the lower ionosphere, *Proc. Int. Conf. Ionos.*, 484.

Molchanov, O. A., M. M. Mogilevsky, V. V. Afonin, Z. Klos, M. Hayakawa, and N. Shima (1997), Nonlinear ELF-VLF effects observed on Activny satellite, in *Nonlinear Waves and Chaos in Space Plasmas*, edited by T. Hada and H. Matsumoto, chap. 10, p. 337, Terra Sci., Tokyo.

Muldrew, D. G. (1969), Nonvertical propagation and delayed-echo generation observed by the topside sounders, *Proc. IEEE*, *57*, 1097.

Nsumei, P. A., X. Huang, B. W. Reinisch, P. Song, V. M. Vasyliunas, J. L. Green, S. F. Fung, R. F. Benson, and D. L. Gallagher (2003), Electron density distribution over the northern polar region deduced from IMAGE/radio plasma imager sounding, *J. Geophys. Res.*, *108*(A2), 1078, doi:10.1029/2002JA009616.

Ohnami, S., M. Hayakawa, T. F. Bell, and T. Ondoh (1993), Nonlinear wave-wave interactions in the subauroral ionosphere on the basis of ISIS-2 satellite observations of Siple station VLF signals, *Geophys. Res. Lett.*, *20*, 739.

Persoon, A. M. (1988), Electron density distributions in the high-latitude magnetosphere, *Adv. Space Res.*, *8*(8), 79.

Persoon, A. M., D. A. Gurnett, and S. D. Shawhan (1983), Polar cap electron densities from DE 1 plasma wave observations, *J. Geophys. Res.*, *88*, 10,123.

Persoon, A. M., D. A. Gurnett, W. K. Peterson, J. H. Waite Jr., J. L. Burch, and J. L. Green (1988), Electron density depletions in the nightside auroral zone, *J. Geophys. Res.*, *93*, 1871.

Rastani, K., U. S. Inan, and R. A. Helliwell (1985), DE 1 observations of Siple transmitter signals and associated sidebands, *J. Geophys. Res.*, *90*, 4128.

Reinisch, B. W., et al. (2000), The Radio Plasma Imager investigation on the IMAGE spacecraft, *Space Sci. Rev.*, *91*, 319.

Schunk, R. W., and A. F. Nagy (2000), *Ionospheres: Physics, Plasma Physics, and Chemistry*, Cambridge Univ. Press, New York.

Siren, J. C. (1975), Fast hisslers in substorms, *J. Geophys. Res.*, *80*, 93.

Smith, A. J., D. L. Carpenter, and U. S. Inan (1985), Whistler-triggered VLF noise bursts observed on the DE-1 satellite and simultaneously at Antarctic ground stations, *Ann. Geophys.*, *3*, 81.

Smith, R. L. (1960), Guiding of whistlers in a homogeneous medium, *J. Res. Natl. Bur. Stand. U.S., Sect. D*, *64*(5), 505.

Smith, R. L., and J. J. Angerami (1968), Magnetospheric properties deduced from OGO 1 observations of ducted and non-ducted whistlers, *J. Geophys. Res.*, *73*, 1.

Sojka, J. J., L. Zhu, M. David, and R. W. Schunk (2000), Modeling the evolution of meso-scale ionospheric irregularities at high latitudes, *Geophys. Res. Lett.*, *27*, 3595.

Sonwalkar, V. S. (1995), Magnetospheric LF- VLF-, and ELF-waves, in *Handbook of Atmospheric Electrodynamics*, edited by H. Volland, p. 407, CRC Press, Boca Raton, Fla.

Sonwalkar, V. S. (1999), Whistlers, in *Encyclopedia of Electrical and Electronic Engineering*, vol. 23, edited by J. G. Webster, p. 580, John Wiley, Hoboken, N. J.

Sonwalkar, V. S., and J. Harikumar (2000), An explanation of ground observations of auroral hiss: Role of density depletions and meter-scale irregularities, *J. Geophys. Res.*, *105*, 18,867.

Sonwalkar, V. S., and U. S. Inan (1986), Measurements of Siple transmitter on the DE 1 satellite: Wave normal direction and antenna effective length, *J. Geophys. Res.*, *91*, 154.

Sonwalkar, V. S., and U. S. Inan (1989), Lightning as an embryonic source of VLF hiss, *J. Geophys. Res.*, *94*, 6986.

Sonwalkar, V. S., T. F. Bell, R. A. Helliwell, and U. S. Inan (1984), Direct multiple path magnetospheric propagation: A fundamental property of nonducted VLF waves, *J. Geophys. Res.*, *89*, 2823.

Sonwalkar, V. S., U. S. Inan, T. F. Bell, R. A. Helliwell, O. A. Molchanov, and J. L. Green (1994), DE 1 VLF observations during ACTIVNY wave injection experiments, *J. Geophys. Res.*, *99*, 6173.

Sonwalkar, V. S., U. S. Inan, and T. F. Bell (1995), An interpretation of a mysterious 3.0- to 4.6-kHz emission band observed on Voyager 2 near Neptune, *J. Geophys. Res.*, *100*, 1795.

Sonwalkar, V. S., et al. (2000), Initial observations and analysis of whistler-mode echoes received by RPI on IMAGE, *Eos Trans. AGU*, *81*, 48.

Sonwalkar, V. S., X. Chen, J. Harikumar, D. L. Carpenter, and T. F. Bell (2001), Whistler-mode wave injection experiments in the plasmasphere with a radio sounder, *J. Atmos. Sol. Terr. Phys.*, *63*, 1199.

Stix, T. H. (1962), *The Theory of Plasma Waves*, 283 pp., McGraw-Hill, New York.

Tanaka, Y., D. Lagoutte, M. Hayakawa, and F. Lefeuvre (1987), Spectral broadening of VLF transmitter signals and sideband structure observed on Aureol-3 satellite at middle latitudes, *J. Geophys. Res.*, *92*, 7551.

Thorne, R. M., E. J. Smith, R. K. Burton, and R. E. Holzer (1973), Plasmaspheric hiss, *J. Geophys. Res.*, *78*, 1581.

Timleck, P. L., and G. L. Nelms (1969), Electron densities less than 100 electrons cm-3 in the topside ionosphere, *Proc. IEEE*, *57*, 1164.

Titova, E. E., V. I. Di, V. E. Yurov, O. M. Raspopov, V. Y. Trakhtengertz, F. Jiricek, and P. Triska (1984), Interaction between VLF waves and turbulent ionosphere, *Geophys. Res. Lett.*, *11*, 323.

Tsyganenko, N. A., and D. P. Stern (1996), Modeling the global magnetic field and the large-scale Birkeland current system, *J. Geophys. Res.*, *101*, 27,187–27,198.

Wang, T. N. C. (1970), VLF input impedance characteristics of an electric antenna in a magnetoplasma, *Tech. Rep. 3414-1*, Radiosci. Lab. Stanford Electron. Lab., Stanford Univ., Stanford, Calif.

Wang, T. N. C., and T. F. Bell (1972), VLF/ELF input impedance of an arbitrarily oriented loop antenna in a cold collisionless plasma, *IEEE Trans. Antennas Propag.*, *20*(3), 394.

T. F. Bell, D. L. Carpenter, and U. S. Inan, Space, Telecommunications, and Radioscience Laboratory, Packard Building, Stanford University, Stanford, CA 94305-9515, USA. (bell@nova.stanford.edu; dlc@nova.stanford.edu; inan@nova.stanford.edu)

R. F. Benson, NASA Goddard Space Flight Center, Code 692, Greenbelt, MD 20771, USA. (robert.f.benson@nasa.gov)

X. Chen, P.O. Box 211353, Auke Bay, AK 99821, USA. (xiangdongc@hotmail.com)

J. Harikumar, Physical Science Laboratory, New Mexico State University, Las Cruces, NM 88003, USA. (jai_harikumar@yahoo.com)

J. Li, V. S. Sonwalkar, and A. Venkatasubramanian, Department of Electrical and Computer Engineering, University of Alaska Fairbanks, 306 Tanana Drive, Room 203, Duckering Building, Fairbanks, AK 99775-5915, USA. (fsjl3@uaf.edu; ftav@uaf.edu; ffvss@uaf.edu)

B. W. Reinisch, Center for Atmospheric Research, University of Massachusetts, 600 Suffolk Street, Lowell, MA 01845, USA. (bodo_reinisch@uml.edu)

M. A. Spasojević, Space Physics Research Group, Space Science Laboratory, University of California, 7 Gauss Way, Berkeley, CA 94720-7450, USA. (maria@ssl.berkeley.edu)

W. W. L. Taylor, QSS Group, Inc., NASA Goddard Space Flight Center, Code 630, Greenbelt, MD 20771, USA. (taylor@mail630.gsfc.nasa.gov)